The Giant Vesicle Book, ed. by R. Dimova and C. Marques (CRC Press, 2019)

5 Understanding giant vesicles: A theoretical perspective

Reinhard Lipowsky

As simple as possible but not simpler.

Albert Einstein

Contents

5.1 INTRODUCTION AND OVERVIEW

The architecture of biological membranes is characterized by a wide range of length scales. On the μm scale, these membranes exhibit a unique combination of properties: (i) They form closed surfaces without edges; (ii) They are highly flexible and, thus, can easily adapt their shape to external perturbations; (iii) In spite of this flexibility, they provide robust and stable barriers between the different aqueous compartments; and (iv) In the cell, these compartments are continuously remodeled via membrane fusion and fission (or scission).

These properties arise from the specific molecular structure of these membranes. When viewed on the nm scale, each biomembrane consists of a specific mixture of many different lipids and membrane proteins which reflects the biological functions of this membrane. However, in spite of this chemical complexity, all biomembranes are organized according to the same universal principle: their basic building block is provided by a *bilayer of lipid molecules*. The latter molecules are essentially *insoluble* in the aqueous solution which ensures the stability of the membrane. In addition, these lipid bilayers are maintained in a *fluid* state which enables the membranes to adapt to external perturbations by remodeling of membrane composition, shape, and topology.

Many of the fascinating remodeling processes that have been found for biological membranes can also be observed for giant unilamellar vesicles (GUVs) that are formed by membranes with a relatively small number of molecular components. The theory described here will typically be compared to experimental observations on lipid vesicles but the same theory applies to vesicle membranes that are composed of lipids and membrane proteins.

One intriguing example for the remodeling of membrane shape is provided by the formation of membrane necks via budding, a crucial step of all endo- and exocytotic processes. Another example is provided by the formation of membrane nanotubes, highly curved membrane structures that protrude from weakly curved membrane segments. As far as the remodeling of composition is concerned, we now have a variety of lipid mixtures that can phase separate into two fluid phases, a liquid-ordered and a liquid-disordered phase. When we study this membrane phase separation in giant vesicles, we often observe large intramembrane domains that partition the vesicle membrane into a few membrane compartments with a lateral extension in the micrometer range. In addition, multicomponent membranes exposed to a heterogeneous environment form ambience-induced segments that can also differ

in their molecular composition. One example for this type of segmentation is provided by vesicle membranes exposed to aqueous two-phase systems or water-in-water emulsions which exhibit several wetting morphologies. The interplay between ambience-induced segmentation and membrane phase separation leads to the confinement of phase separation to single membrane segments which represents a generic mechanism to suppress the formation of large intramembrane domains or rafts in cellular membranes.

The present chapter is organized as follows. The next two Sections 5.2 and 5.3 are introductory in nature: they describe basic aspects of biomembranes and provide an elementary view of membrane curvature. The relation between local curvature generation and spontaneous curvature is explained in Section 5.3.5. Different molecular mechanisms for local curvature generation are described in Box 5.1. Section 5.4 describes the theory of curvature elasticity for uniform membranes.[1] This theory is based on the *local* curvature-elastic properties of the membranes, but also takes into account that the ultralow lipid solubility and the osmotic conditions lead to *global* constraints on the membrane area and the vesicle volume. In fact, what makes this theory both appealing and challenging is this interplay between local and global membrane properties.

We will focus on the spontaneous curvature model but also discuss the modifications arising from area-difference-elasticity. On the one hand, the spontaneous curvature model is particularly attractive from a theoretical point of view because it depends only on a small number of curvature-elastic parameters. In fact, for membranes with a laterally uniform composition, the spontaneous curvature model involves only two such parameters, (i) the bending rigidity κ which describes the resistance of the membrane against bending deformations and (ii) the spontaneous curvature which provides a quantitative measure for the bilayer asymmetry of the membranes. On the other hand, the spontaneous curvature model is also sufficient to obtain a quantitative description for the behavior of many membranes of interest. Indeed, this model applies to all membranes with (at least) one molecular component such as cholesterol that undergoes frequent flip-flops between the two leaflets of the bilayer. Area difference elasticity is only relevant in the absence of flip-flops, i.e., when the number of molecules is separately conserved in each leaflet.

One striking consequence of curvature elasticity is the formation of closed membrane necks that represent narrow funnel-like membrane structures between two larger membrane segments. The stability of these necks depends on the relative magnitude of the neck curvature and the spontaneous curvature, which may contain a nonlocal contribution from area-difference-elasticity. These stability conditions for closed membrane necks can be reinterpreted as effective constriction forces generated by spontaneous curvature. Simple estimates show that sufficiently large spontaneous curvatures lead to the cleavage of the membrane necks and thus to complete membrane fission. The different aspects of membrane necks are summarized in Box 5.2.

[1] Here and below, a 'uniform membrane' is 'laterally uniform' and a 'uniform aqueous phase' is 'spatially uniform'.

Sections 5.5 and 5.6 are devoted to two striking morphologies formed by uniform membranes: (i) multi-sphere shapes that involve small spherical buds and (ii) membrane nanotubes that can be necklace-like or cylindrical. Section 5.7 describes the behavior of vesicles that interact with an adhesive and rigid surface. For simplicity, the latter section will focus on vesicle membranes with a laterally uniform composition but will also discuss adhesion of vesicles as an example for ambience-induced segmentation of membranes. A closely related subject, the behavior of adhesive nanoparticles in contact with membranes and vesicles, will be addressed in Chapter 8 of this book. The shapes and shape transformations of vesicles that contain two or multiple intramembrane domains are discussed in Section 5.8, and the wetting of membranes in contact with aqueous two-phase systems or water-in-water emulsions in Section 5.9. For partial wetting, the water-water interfaces exert capillary forces onto the membranes which then respond with strong shape deformations. On the nanometer scale, the membrane segments close to the three-phase contact line should be curved in a smooth manner and the capillary forces then lead to a complex force balance along this contact line which involves an intrinsic contact angle. On the micrometer scale, the membrane shapes exhibit kinks which define an apparent contact line and apparent contact angles. Experimental aspects of aqueous two-phase systems will be addressed in Chapter 29 of this book. Both membrane phase separation and membrane wetting leads to vesicle membranes that have a laterally nonuniform composition. At the end, we will briefly look at the consequences of curvature elasticity for membrane fusion and fission (or scission) of membranes, the two most important topological transformations of membranes.

Each of the different membrane systems discussed in Sections 5.7 through 5.9 involves one additional parameter: the adhesive strength W of substrate surfaces, the line tension λ of domain boundaries, and the interfacial tension $\Sigma_{\alpha\beta}$ between two different aqueous phases. Because all of these parameters can be measured or deduced from experimental observations, the theory leads to quantitative predictions. In fact, the theory described here leads to a large number of simple relationships between material parameters and geometric quantities which provide important checkpoints for the comparison between theory and experiment.

5.2 BIOMEMBRANES AND GIANT VESICLES: BASIC ASPECTS

Here and below, the term "biomembranes" will be used as an abbreviation for "biological and biomimetic membranes." These two types of membranes differ primarily in their chemical complexity. Biological or cellular membranes usually contain hundreds or even thousands of different lipid species and a large number of different membrane proteins. Biomimetic membranes as considered here have a much simpler composition with only a few molecular components but share one crucial physical property with biological membranes, namely their fluidity, which enables both types of membranes to undergo analogous remodeling processes. The simplest biomimetic membranes are provided by one-component lipid bilayers which have a molecular structure as in Figure 5.1.

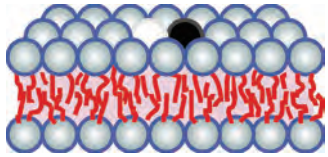

Figure 5.1 Lipid bilayer as the basic building block of all biomembranes: The lipid molecules are arranged into two monolayers or leaflets, with the lipid headgroups forming the two interfaces between the bilayer and the aqueous solutions. The thickness of the bilayer is 4 to 5 nm. For a *fluid* bilayer, each lipid molecule undergoes rapid lateral diffusion within the membrane. This diffusive process is based on the pairwise exchange of neighboring lipids (black and white) on the time scale of nanoseconds.

5.2.1 BIOMEMBRANES BASED ON LIPID BILAYERS

Essentially all biological membranes contain a single lipid bilayer as their basic building block. The importance of lipids was already realized by Langmuir and others at the beginning of the 20th century. This insight came from spreading experiments: the membranes were dissolved in a volatile organic solvent, the solution was spread on a water surface, and the solvent was evaporated. In this way, one obtains a lipid monolayer at the air–water interface. Such a technique was also used by Gorter and Grendel who extracted lipids from red blood cells (Gorter and Grendel, 1925; Robertson, 1960). They found that the area of the monolayer was approximately twice the area of the cell and proposed that the cell should be covered by a lipid bilayer. This proposal was confirmed, in the 1950s and 1960s, by imaging cross-sections of biomembranes via electron microscopy. Such electron microscopy images gave direct evidence that cell membranes are based upon a single bilayer and showed that these bilayers have a thickness of 4–5 nm (Robertson, 1959).

Electron microscopy studies also demonstrated that bilayers are already formed by a single species of phospholipid molecules (Bangham and Horne, 1964). Therefore, bilayers consisting of one or a few lipid components have become important model systems for biological membranes. Different bilayer systems have been developed and intensely studied, including multilamellar liposomes, black lipid membranes, solid-supported bilayers, and unilamellar vesicles. Giant unilamellar vesicles as considered here typically have a linear size of tens of micrometers and can be directly imaged in their fluid state using optical microscopy.

5.2.2 SEMI-PERMEABILITY AND OSMOTIC CONDITIONS

One basic function of biological membranes is that they partition space into separate aqueous compartments and represent effective barriers for the diffusion of ions and solute molecules from one compartment to another. These functions are also provided by lipid bilayers. When these bilayers form vesicles, they create an interior aqueous compartment that is well separated from the exterior solution. Indeed, the bilayers are permeable to small uncharged molecules such as H_2O, O_2, and CO_2 as well as H_3O^+ and OH^- ions, but do not allow the permeation of other ions or larger water-soluble molecules such as glucose and other monosaccharides. As a consequence, these solutes represent osmotically active "particles" and exert osmotic pressures onto the vesicle membranes. The experimental methods to measure the permeability of membranes are reviewed in Chapter 20 of this book.

The osmotic pressures depend on the solute concentrations in the interior and exterior solutions. If a vesicle membrane is exposed to different interior and exterior concentrations, the resulting osmotic pressure difference causes water to move through the membrane into the compartment with the higher solute concentration. First, consider a higher solute concentration in the exterior solution which leads to osmotic deflation of the vesicle. In this case, the water outflux reduces the vesicle volume until the interior particle concentration matches the exterior one and the osmotic pressure difference is close to zero. On the other hand, if we start with a higher solute concentration in the interior compartment, the volume of the vesicle is increased by osmotic inflation. However, this volume increase is truncated by the limited ability of the vesicle membrane to increase its area by mechanical stretching. Indeed, when a lipid bilayer is mechanically stretched, its area can only be increased by a few percent before it ruptures. Therefore, once the inflated vesicle has attained a spherical shape, further influx of water increases the membrane tension up to a limiting value at which the membrane ruptures and forms pores. These pores then provide an alternative pathway for the reduction of the osmotic pressure difference.

5.2.3 FLUIDITY OF BIOMEMBRANES

Another universal aspect of biological membranes is that they are maintained in a fluid state which is characterized by fast lateral diffusion of the molecules along the membrane. This membrane fluidity became generally accepted at the beginning of the 1970s as a result of three parallel developments. First, the lateral diffusion was probed by spin-labeled lipids (Kornberg and McConnell, 1971; Devaux and McConnell, 1972) and steroids (Sackmann and Träuble, 1972; Träuble and Sackmann, 1972) which led to lateral diffusion constants of the order of 1 μm^2 per second. Nowadays, the lateral diffusion of membrane molecules can be observed directly by fluorescence recovery after photobleaching (FRAP) (Almeida and Vaz, 1995) and by single particle tracking (Sako and Kusumi, 1994; Saxton and Jacobson, 1997; Fujiwara et al., 2002; Kusumi et al., 2005), two methods that have been applied to a large variety of biomimetic and biological membranes. These studies confirmed that the lateral diffusion constants of membrane molecules are indeed of the order of 1 μm^2 per second. A detailed discussion of both FRAP and single particle tracking as well as tables with diffusion constants for a variety of lipids can be found in Chapter 21 of this book.

Second, it has been realized that the observed shape transformations of red blood cells (Canham, 1970; Evans, 1974) and lipid vesicles (Helfrich, 1973; Deuling and Helfrich, 1976) are only possible if the membranes represent two-dimensional liquids. Indeed, these shape transformations change the curvature of the membranes in a smooth and continuous manner and would be impossible for solid-like or polymerized membranes. Particularly interesting shape changes are provided by budding processes in

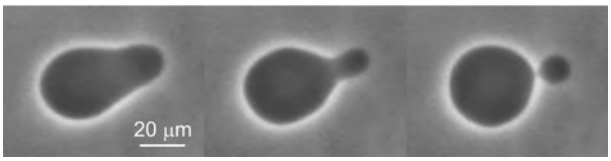

Figure 5.2 Formation of a spherical out-bud from a giant unilamellar vesicle (GUV) as observed by phase contrast microscopy. This budding process, which took about 5 s, proceeds in a smooth and continuous manner and provides direct evidence on the micrometer scale that the lipid membrane is in a fluid state on the molecular scale. (Reproduced with permission from Dimova, R. et al., A practical guide to giant vesicles: Probing the membrane nanoregime via optical microscopy, *J. Phys. Cond. Mat.*, 18, S1151–S1176, 2006, Institute of Physics)

which small spherical out- or in-buds are formed from larger mother vesicles. Out-buds point towards the exterior aqueous solution, in-buds towards the interior solution. One example for the formation of an out-bud is shown in Figure 5.2. Such a budding process provides direct evidence that the membrane is in a fluid state. The associated curvature elasticity of biomembranes has now been developed into a quantitative theory (Berndl et al., 1990; Seifert and Lipowsky, 1990; Seifert et al., 1991; Miao et al., 1991; Lipowsky, 1991; Miao et al., 1994; Döbereiner et al., 1997; Lipowsky, 2013; Liu et al., 2016; Lipowsky, 2018a) which will be described in this chapter.

Third, in 1972, a large body of observations on cellular membranes was integrated into the fluid mosaic model in which the membrane proteins are dispersed in a fluid bilayer of lipids (Singer and Nicolson, 1972). Whether the fluid mosaic model actually describes the supramolecular structure of cell membranes has been a matter of some debate. On the one hand, the endocytosis and exocytosis of cell membranes involves the formation of fluid domains that are enriched in membrane-anchored receptors and coat proteins and can be understood in terms of domain-induced budding (Lipowsky, 1992, 1993; Agudo-Canalejo and Lipowsky, 2015a).

On the other hand, it has also been proposed that cell membranes contain intramembrane domains, so-called rafts, that are enriched in certain lipids such as sphingomyelin and cholesterol (Simons and Ikonen, 1997). In spite of a large number of experimental studies, including superresolution microscopy methods such as stimulated emission depletion (STED) microscopy, it has not possible to obtain direct evidence for such rafts in cellular membranes. If these lipid rafts exist in mammalian cells, their diameter does not exceed 20 nm (Eggeling et al., 2009). The different experimental techniques used to search for such rafts have been critically reviewed by (Klotzsch and Schütz, 2013). One generic mechanism that explains the difficulty to observe membrane phase separation in cellular membranes is ambience-induced segmentation by the heterogeneous environment to which these membranes are exposed (Lipowsky, 2014b) as discussed in Section 5.8.5 below.

5.2.4 REMODELING OF COMPOSITION AND SHAPE

In general, the fluidity of biomembranes implies that these membranes can easily adapt to changes in their environment by remodeling their composition, shape, and topology. This multi-responsive behavior includes shape transformations of GUVs, membrane segmentation by laterally nonuniform environments such as adhesive surfaces, membrane phase separation, and the responses of GUVs to capillary forces arising from water-in-water droplets.

The remodeling of membrane composition in ternary lipid mixtures leads to the nucleation and growth of intramembrane domains that can be directly observed in the optical microscope, see Figure 5.3. Such domains, which demonstrate the coexistence of two (or more) lipid phases, have now been observed for a variety of membrane systems including giant vesicles (Dietrich et al., 2001; Veatch and Keller, 2003; Baumgart et al., 2003; Bacia et al., 2005; Riske et al., 2006; Dimova et al., 2007; Semrau et al., 2008), solid-supported membranes (Jensen et al., 2007; Garg et al., 2007; Kiessling et al., 2009), hole-spanning (or black lipid) membranes (Collins and Keller, 2008), as well as pore-spanning membranes (Orth et al., 2012). The phase diagrams of such three-component membranes have been determined using spectroscopic methods (David et al., 2009) as well as fluorescence microscopy of giant vesicles and X-ray diffraction of membrane stacks (Veatch et al., 2006; Vequi-Suplicy et al., 2010; Uppamoochikkal et al., 2010; Pataraia et al., 2014). The experimental aspects of lipid phase separation and domain formation are reviewed in more detail in Chapter 18 of this book.

Another particularly striking example for the remodeling of membrane shape that does not require membrane phase separation is provided by the spontaneous tubulation of GUVs (Li et al., 2011; Lipowsky, 2013; Liu et al., 2016). Two examples for the resulting pattern of nanotubes are displayed in Figure 5.4. In these examples, the vesicles respond to osmotic deflation by the formation of many nanotubes that emanate from the giant mother vesicle and protrude into the vesicle interior. As a result, highly curved membrane segments coexist with weakly curved segments even though the membrane has a laterally uniform composition. The nanotubes shown in Figure 5.4 were formed spontaneously, i.e., in the absence of external pulling forces. Another quite different mechanism for the formation of membrane

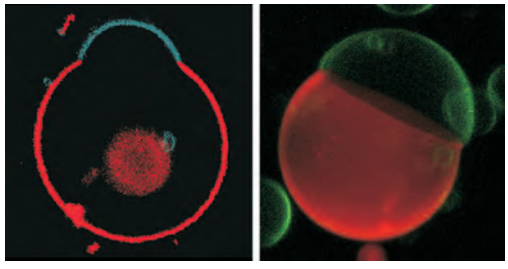

Figure 5.3 Remodeling of membrane composition can lead to domain-induced budding of vesicles as theoretically predicted in (Lipowsky, 1992, 1993; Jülicher and Lipowsky, 1993) and observed by fluorescence microscopy in (Baumgart et al., 2003; Riske et al., 2006): (left) Cross section through a vesicle that formed two domains after a decrease in temperature (Baumgart et al., 2003); and (right) Three-dimensional confocal scan of a two-domain vesicle that was formed by electrofusion. In both cases, the vesicle membrane is composed of dioleoyl phosphadityl choline (DOPC), sphingomyelin, and cholesterol (see Appendix 1 of the book for structure and data on these lipids) together with small concentrations of two fluorescent probes. (Reproduced with permission from Riske, K.A. et al., *Biophys. Rev. Lett.*, 1, 387–400, 2006. Copyright (c) 2006 World Scientific Publishing.)

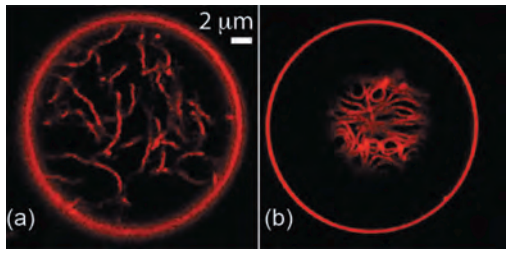

Figure 5.4 Remodeling of membrane shape can lead to complex patterns of flexible nanotubes. The nanotubes were formed by liquid-disordered membranes after the interior aqueous compartment separated into a PEG-rich and dextran-rich phase: (a) Disordered pattern corresponding to a vesicle membrane that is completely wetted by the PEG-rich phase; and (b) Layer of densely packed tubes corresponding to a membrane that is partially wetted by both aqueous phases. All tubes are connected to the outer vesicle membranes (red circles). In both images, the diameter of the tubes is below the diffraction limit of the confocal microscope but the tubes are theoretically predicted to be necklace-like and cylindrical in (a) and (b), respectively (Liu et al., 2016). (Reproduced with permission from Liu, Y. et al., *ACS Nano*, 10, 463–474, 2016. Copyright American Chemical Society.)

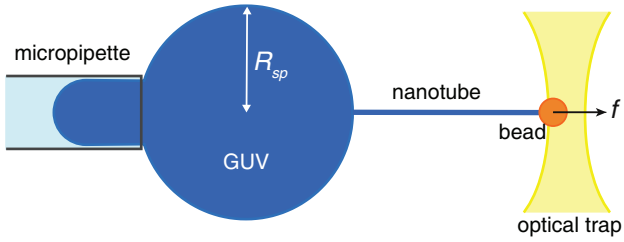

Figure 5.5 Pulling a membrane nanotube attached to a bead from a giant unilamellar vesicle (GUV) by an optical trap: The weakly curved GUV is aspirated by the micropipette, the right end of the strongly curved nanotube experiences the pulling force *f* arising from the optical trap. The latter force is typically of the order of 10 pN and can then generate tubes with a radius of 10–20 nm.

nanotubes is provided by external pulling forces that are locally applied to the membranes. A particularly instructive setup for the latter tubulation process is obtained if one aspirates a giant unilamellar vesicle in a micropipette and simultaneously applies a pulling force to a membrane-bound nanobead via magnetic tweezers (Heinrich and Waugh, 1996) or optical traps (Sorre et al., 2012), as schematically depicted in Figure 5.5.

The experimental methods that have been developed for GUVs composed of a few lipid components can also be applied to giant plasma membrane vesicles (GPMVs) or "blebs," which contain a wide assortment of different lipids and proteins, all oriented in the same way as in the original cell membrane. In spite of their chemical complexity, the membranes of GPMVs were found to phase separate into coexisting lipid phases (Baumgart et al., 2007; Veatch et al., 2008), in close analogy to ternary lipid mixtures. One cellular process that has been elucidated using GPMVs is the molecular recognition of "self" during phagocytosis by macrophages. This recognition process involves the binding of the immunoglobulin CD47, a ubiquitous "marker of self" protein, to the macrophage receptor SIRPα (Sosale et al., 2015). The adhesion of GPMVs with CD47 to SIRPα immobilized on a substrate surface revealed that the two proteins bind in a cooperative manner (Steinkühler et al., 2019), confirming previous theoretical studies (Weikl et al., 2009, 2016; Hu et al., 2013). Furthermore, it has also been observed that GPMVs form many nanotubes under deflation and that these tubulated vesicles exhibit rather unusual elastic properties (Steinkühler et al., 2018b).

5.2.5 STABILITY OF BILAYER MEMBRANES

In spite of their high flexibility, lipid membranes have a robust molecular architecture and maintain this architecture even under strong local deformations. One example is provided by force-induced tubulation as shown in Figure 5.5. Using this method, one can produce nanotubes or "tethers" with a radius of only 10 nm, which should be compared to the bilayer thickness of 4–5 nm (Sorre et al., 2012). Tubes of a similar width have also been generated by a slightly different setup in which the laser trap is replaced by another micropipette that grabs the nanobead (Hochmuth et al., 1982; Tian et al., 2009). However, in spite of the large curvature of these nanotubes, the tube membranes maintain their structural integrity and provide an efficient separation of the interior and exterior aqueous compartments. Detailed information about the experimental method to pull nanotubes from GUVs can be found in Chapter 16 of this book.

The stability of the bilayer structure reflects the ultralow solubility of phospholipids in water. One measure for this solubility is provided by the critical micelle concentration which represents both the concentration at which the lipids start to self-assemble into bilayers (instead of micelles) and the concentration of individual lipid molecules in the presence of bilayers. The critical micelle concentration of phospholipids decreases exponentially with their chain length, i.e., with the number of hydrocarbon groups per chain (Cevc and Marsh, 1987). The phospholipid dimyristoyl phosphatidyl choline (DMPC, see Appendix 1 of the book for structure and data on this and other lipids), for example, has the relatively short chain length of 14 hydrocarbon groups, but its critical micelle concentration is only $10^{-10.5}$ in mole fraction units or about 0.95 DMPC molecules per μm^3. When this lipid forms a giant unilamellar vesicle with a radius of 10 µm, the vesicle membrane consists of about 4×10^9 lipid molecules whereas the interior aqueous compartment of the vesicle contains only about 4×10^3 such molecules. Most biologically relevant phospholipids have a chain length that exceeds 14 hydrocarbon groups which implies an even lower critical micelle concentration. As a consequence, one can usually ignore any exchange of phospholipids between the bilayer membrane and the aqueous solutions and assume that the membrane contains a fixed number of such lipids.

5.2.6 POLYMORPHISM OF VESICLES

Because biomembranes are fluid, one might expect that their shape can be understood by analogy with liquid droplets. However, in the absence of external forces or constraints, a liquid droplet of a given volume always attains a spherical shape in order to minimize its interfacial area and, thus, its interfacial free energy. In contrast to liquid droplets, lipid vesicles can attain a large variety of different shapes such as discocytes, stomatocytes, and dumbbells. Furthermore, the vesicle may undergo shape transformations as one changes the osmotic conditions or the temperature. Because the lipid molecules are practically insoluble in water, the total number of lipid molecules within

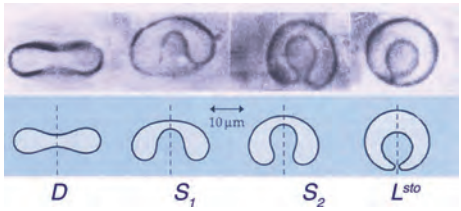

Figure 5.6 Temperature-induced shape transformation of a single vesicle: In this example, the vesicle starts from the initial shape of a discocyte (*D*) which is transformed, via the intermediate stomatocytes S_1 and S_2, into the limit shape L^{sto} consisting of two spheres. The small sphere of L^{sto} forms an in-bud that is connected to the large sphere via a closed membrane neck. The generation of a smooth spherical bud without any membrane folds again demonstrates the fluidity of the membrane. The top row displays images of phase contrast microscopy, the bottom row theoretical shapes with minimal curvature energy. (From Berndl, K. et al., *Europhys. Lett.*, 13, 659–664, 1990.)

the membrane is conserved during such shape transformations. In addition, at any given temperature, each lipid molecule tries to occupy a certain optimal area within the membrane. Furthermore, when exposed to external forces or constraints, lipid bilayers hardly change their area before they rupture. Therefore, the area of the vesicle membrane is conserved, to a very good approximation, during isothermal shape transformations arising, e.g., from osmotic deflation and inflation. The latter processes change the vesicle volume for fixed membrane area. In general, the volume of a vesicle can become arbitrarily small but cannot exceed the volume of a sphere.

Shape transformations can also be induced by temperature changes reflecting the different thermal expansivities of the lipid bilayer and the aqueous solution. When we increase the temperature by ΔT, the initial membrane area A_0 increases by $\Delta A = \alpha_A \Delta T A_0$ with $\alpha_A \simeq 2 \times 10^{-3}$/K for lipid bilayers. At the same time, the initial water volume V_0 increases by $\Delta V = \alpha_V \Delta T V_0$ with $\alpha_V \simeq 2 \times 10^{-4}$/K. When we apply these relations to a GUV, we find that an increase in temperature generates excess area of the membrane and reduces the volume-to-area ratio of the vesicle. One example for temperature-induced shape transformations is displayed in Figure 5.6.

The multi-responsive behavior of GUVs as illustrated by Figures 5.2 through 5.6 can be understood, in a quantitative manner, by the unusual curvature-elastic properties of the vesicle membranes. In the next two sections, we will first discuss the general concept of membrane curvature and then introduce the spontaneous curvature model for the description of curvature elasticity.

5.3 CURVATURE OF MEMBRANES

This section provides an elementary introduction into different aspects of curvature. It first emphasizes that membrane curvature emerges on nanoscopic scales and then describes basic concepts from differential geometry which include the two principal curvatures, the mean curvature, and the Gaussian curvature. Furthermore, one simple but important issue that is discussed in some detail is our convention for the sign of the principal curvatures, which can be positive or negative. At the end of this section, several molecular mechanisms for local curvature generation are briefly discussed and summarized in Box 5.1. Local curvature generation is intimately related to the preferred or spontaneous curvature of a membrane. The latter curvature can again be positive or negative. The present section is supplemented by Appendix 5.A on differential geometry.

5.3.1 EMERGENCE OF CURVATURE ON NANOSCOPIC SCALES

As shown in Figure 5.3 and Figure 5.6, vesicle shapes appear to be rather smooth when viewed under the optical microscope. Therefore, on the micrometer scale, membranes can be described as smoothly curved surfaces and then characterized by their curvature. However, this smoothness does not persist to molecular scales, i.e., when we resolve the molecular structure of a bilayer membrane as in Figure 5.7.

Because membranes are immersed in liquid water, each lipid and protein molecule undergoes thermal motion with displacements both parallel and perpendicular to the membrane. The perpendicular displacements represent molecular protrusions that roughen the two interfaces bounding the membrane. Therefore, in order to characterize a lipid/protein bilayer by its curvature, one has to consider small membrane patches and average over the molecular conformations within these patches. The minimal lateral size of these patches can be determined from the analysis of the bilayer's shape fluctuations and was found, from molecular dynamics simulations of a one-component lipid bilayer, to be about 1.5 times the membrane thickness, see Figure 5.7 (Goetz et al., 1999). For a membrane with a thickness of 4 nm, this minimal size is about 6 nm. Because such a membrane patch contains 80–100 lipid molecules, membrane curvature should be regarded as an emergent property arising from the collective behavior of a large number of lipid molecules.

The curvature just discussed applies to the midsurface of the bilayer membrane, i.e., to the surface between the two leaflets of the bilayer. Furthermore, for a membrane segment with midsurface area A and bending rigidity κ, curved conformations as in Figure 5.7 are only possible if the membrane is "tensionless" in the sense that the mechanical membrane tension is small compared to κ/A (Goetz and Lipowsky, 1998). For the example displayed in Figure 5.7, the latter tension scale is found to be $\kappa/A = 0.08$ mN/m.

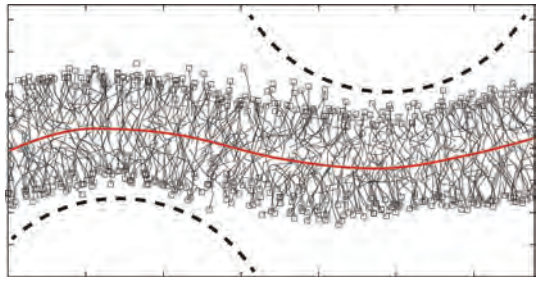

Figure 5.7 Emergence of membrane curvature on nanoscopic scales as observed in molecular dynamics simulations. The bilayer has a thickness of about 4 nm, the smallest curvature radius of its midsurface (red curve) is about 6 nm. For comparison, two circles (broken lines) with a radius of 6 nm are also displayed. (Reproduced from Goetz, R. et al., *Phys. Rev. Lett.*, 82, 221–224, 1999.)

5.3.2 MEAN AND GAUSSIAN CURVATURE

For each point on a smooth surface, we can construct a unit normal vector perpendicular to the membrane surface. Now, any plane that contains both the chosen point and this normal vector, defines a so-called normal section of the membrane surface, see Figure 5.8. The intersection between the surface and such a normal section defines a cross-sectional curve through the chosen point with a certain curvature C at this point. I will take this curvature to be positive if the cross-sectional curve bulges in the direction of the chosen normal vector as in Figure 5.8. This sign convention ensures that the cross-sectional curves on a sphere have positive curvature. Now, let us rotate the normal section around the normal vector. As a result of this rotation, the cross-sectional curve through the chosen point changes and so does the curvature C. As we change the rotation angle from 0 to 360 degrees, the latter curvature varies over a certain range as given by $C_{\min} \leq C \leq C_{\max}$. The two extremal values $C_{\min}$ and $C_{\max}$ define the principal curvatures, C_1 and C_2, at the chosen point. These principal curvatures correspond to the eigenvalues of the negative curvature tensor, see Appendix 5.A. Furthermore, for $C_1 \neq C_2$, the normal sections that contain the cross-sectional curves with $C = C_1$ and $C = C_2$ are always orthogonal to each other.

For fluid membranes as considered here, the molecules diffuse laterally along the membrane, which implies that the membrane surface should be described in terms of geometric quantities that do not depend on the choice of the surface coordinates, i.e., that are invariant under a reparametrization of the surface. Such quantities are provided, apart from a possible change of sign, by the principal curvatures C_1 and C_2 or equivalently by the mean curvature

$$M \equiv \frac{1}{2}(C_1 + C_2) \tag{5.1}$$

and the Gaussian curvature

$$G \equiv C_1 C_2. \tag{5.2}$$

The mean curvature is proportional to the trace of the curvature tensor whereas the Gaussian curvature is equal to its determinant (Appendix 5.A). Note that $C_1 = M - \sqrt{M^2 - G}$ and $C_2 = M + \sqrt{M^2 - G}$. Both expressions are always real-valued because $M^2 \geq G$.[2] Indeed, the latter inequality is equivalent to $(C_1 - C_2)^2 \geq 0$ and, thus, holds for any shape of the membrane segment. The equality $M^2 = G$ applies to spherical segments with $C_1 = C_2$.

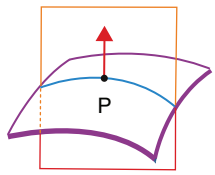

Figure 5.8 Normal section through membrane surface: Consider a point P of the membrane surface and the normal vector (arrow) at point P. A normal section is provided by any plane that contains both the point P and its normal vector. The intersection between the chosen normal section and the membrane surface defines a cross-sectional curve through point P. This curve has a certain curvature at point P. The latter curvature changes in a smooth manner as we rotate the normal section around the normal vector.

[2] The expressions for C_1 and C_2 imply that $C_1 = \dot{\psi}$ and $C_2 = \sin\psi / r$ for axisymmetric shapes parametrized by the tilt angle ψ and the radial coordinate r of the shape contour (Seifert et al., 1991).

5.3.3 SIGN OF MEMBRANE CURVATURE

The mean curvature M is invariant under all orientation-preserving transformations of the surface coordinates, i.e., under all transformations that have a positive Jacobi determinant. The latter transformations do not affect the normal vectors of the membrane. However, we may also consider improper transformations of the surface coordinates which reverse the orientation of the normal vectors. A simple example of such an improper transformation A^1 is provided by a transposition of the two surface coordinates, i.e., by the transformation from (s^1, s^2) to $(\bar{s}^1 \equiv s^2, \bar{s}^2 \equiv s^1)$. The reversal of the normal vector implies that the principal curvatures change their sign and so does the mean curvature.

On the one hand, the reversal of the normal vectors provides a useful operation from a theoretical point of view because many physical properties of the membrane should not depend on our choice for the orientation of the normal vectors and must therefore be invariant under the reversal of these vectors. On the other hand, in order to avoid any ambiguity, we need a convention that always assigns a definite orientation to the normal vectors. For vesicle membranes as considered here, we can always distinguish between an interior and an exterior compartment and, thus, can always take the normal vectors to point towards the outer leaflet which is in contact with the exterior aqueous compartment, see Figure 5.9.

The sign of the mean curvature M depends on the sign of the principal curvatures C_1 and C_2. As explained before, each principal curvature is obtained from a certain normal section and taken to be positive if the corresponding cross-sectional curve bulges in the direction of the normal vector. If all cross-sectional curves of the membrane bulge into the direction of the normal vector as in Figures 5.8 and 5.9a, both C_1 and C_2 are positive which implies that the mean curvature M is positive as well.[3] Likewise, the mean

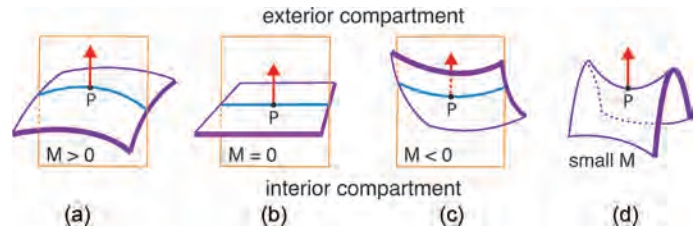

Figure 5.9 Sign convention for mean curvature M: (a) The mean curvature is *positive* if the membrane curves or bulges locally towards its outer leaflet in contact with the exterior compartment; (b) The mean curvature vanishes for a planar membrane; (c) The mean curvature is *negative* if the membrane curves or bulges locally towards its inner leaflet in contact with the interior compartment; and (d) If P is a saddle point, the two principal curvatures C_1 and C_2 have opposite sign and the mean curvature $M = \frac{1}{2}(C_1 + C_2)$ is small or even zero.

[3] Choose local Cartesian coordinates (x,y,z) with the origin given by point $P = (0,0,0)$, normal vector $\hat{n} = (0,0,1)$, and the x-coordinate parallel to the normal section that contains the cross-sectional curve with the principal curvature $C_1 = C_{\min}$. The cross-sectional curves within the normal sections with $y = 0$ and $x = 0$ are then described by $z \approx -C_1 x^2$ and $z \approx -C_2 y^2$ for small values of x and y.

curvature M is *negative* if all cross-sectional curves of the membrane bulge into the direction of the negative normal vector, see Figure 5.9c. At a saddle point of the membrane surface, the two principal curvatures have opposite signs and the mean curvature M can be positive or negative or even vanish, depending on the relative magnitude of the two principal curvatures, see Figure 5.9d.

5.3.4 CONSTANT-MEAN-CURVATURE SHAPES

In general, the principal curvatures and the mean curvature M are local quantities that vary along the membrane surface. Some particularly simple shapes are, however, characterized by constant mean curvature, i.e., all points on the surface have the same mean curvature, see Figure 5.10. Thus, a planar membrane has vanishing mean curvature, $M = 0$, whereas a sphere with radius R_{sp} has mean curvature $M = 1/R_{sp}$ and $M = -1/R_{sp}$ when its inner leaflet is in contact with the interior and the exterior solution, respectively. Likewise, a cylinder with radius R_{cy} has mean curvature $M = 1/(2R_{cy})$ when the enclosed volume of water belongs to the interior compartment and $M = -1/(2R_{cy})$ when this volume is connected to the exterior compartment. Another simple shape is a catenoid for which each point represents a saddle point with vanishing mean curvature $M = 0$ as depicted in Figure 5.10c.

Cylinders represent possible shapes for membrane nanotubes. Another tube morphology that has been observed are necklace-like tubes as shown in Figure 5.11a. The latter tubes consist of identical spheres connected by closed membrane necks. For spheres with radius R_{sp}, the necklace-like tube has mean curvature $M = 1/R_{sp}$ and $M = -1/R_{sp}$ when the enclosed volume of the tube is connected to the interior and exterior solution, respectively. A necklace-like tube consisting of spheres with radius R_{sp} can be continuously transformed into a cylindrical tube with radius $R_{cy} = \frac{1}{2} R_{sp}$, thereby preserving the value of the mean curvature. This transformation proceeds via a family of intermediate unduloids, all of which have the same mean curvature as the necklace-like and the cylindrical tube. The unduloids consist of lemon-like bulges connected by open necks, see the example in Figure 5.11b. Thus, during the constant-mean-curvature transformation, the closed necks of the necklace-like tube open up and the bulges of the necklace retract until the necks and the bellies have the same radius and form a cylindrical tube.

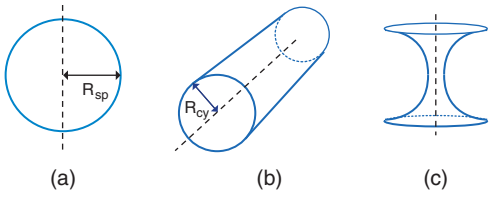

Figure 5.10 Simple membrane shapes with constant mean curvature M: (a) Sphere with radius R_{sp} and mean curvature $M = \pm 1/R_{sp}$; (b) Cylinder with radius R_{cy} and mean curvature $M = \pm 1/(2R_{cy})$; and (c) Catenoid with mean curvature $M = 0$. For spheres and cylinders, the sign of the mean curvature depends on whether the inner leaflet is in contact with the interior or exterior aqueous solution.

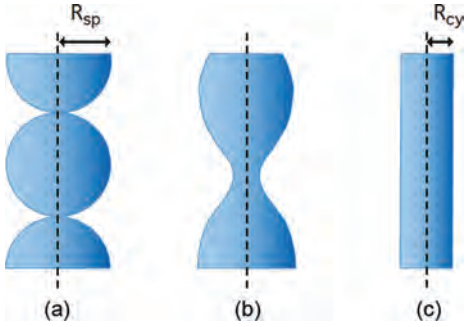

Figure 5.11 Three membrane tubes with different morphologies but the same constant mean curvature M: (a) Necklace-like tube consisting of identical spheres with radius $R_{sp} = 1/|M|$. The spheres are connected by closed membrane necks; (b) Unduloid with lemon-like bulges connected by open necks. The neck radius R_{ne} and the bulge radius R_{bu} are related to $|M|$ via $|M| = 1/(R_{ne} + R_{bu})$; and (c) Cylindrical tube with radius $R_{cy} = 1/(2|M|)$. (Reproduced from Lipowsky, R. *Biol. Chem.* 395, 253–274, 2014b. With permission of Walter de Gruyter GmBH & CO.KG.)

5.3.5 LOCAL CURVATURE GENERATION AND SPONTANEOUS CURVATURE

The simulation snapshot in Figure 5.7 displays a symmetric bilayer consisting of two leaflets that have the same molecular composition and are exposed to the same aqueous environment. Likewise, the cartoons in Figure 5.9 did not indicate any asymmetry between the two leaflets. In real systems, such symmetric bilayers are somewhat exceptional, but they provide a useful reference system because their elastic properties are governed by a single elastic parameter, the bending rigidity κ that provides the basic energy scale of membranes. For phospholipid bilayers, the latter scale is of the order of 10^{-19} J, which is about $20 k_B T$ at room temperature. For different lipid bilayers, the measured values of the bending rigidity vary by about an order of magnitude, see the corresponding tables in Chapters 11, 14, and 15 of this book.

Real bilayer membranes are typically asymmetric. This asymmetry can arise from a different lipid composition of the two leaflets as found in all biological membranes (van Meer et al., 2008; Fadeel and Xue, 2009). One prominent example is provided by the ganglioside GM1, a glycolipid that is abundant in all mammalian neurons (Aureli et al., 2016) and plays an important role in many neuronal processes and diseases (Schengrund, 2015). Furthermore, GM1 acts as a membrane anchor for various toxins, bacteria, and viruses such as the simian virus 40 (Ewers et al., 2010). The curvature generated by different leaflet concentrations of GM1 has been recently studied, both experimentally for giant vesicles (Bhatia et al., 2018; Dasgupta et al., 2018) and by simulations of molecular bilayers (Dasgupta et al., 2018; Sreekumari and Lipowsky, 2018; Miettinen and Lipowsky, 2019). Likewise, membrane proteins in biological membranes have a preferred orientation, which also contributes to their asymmetry. In addition, membranes can acquire such an asymmetry from their environment as provided by the exterior and interior aqueous compartments. Indeed, the membranes become asymmetric when these two compartments contain different concentrations of ions, small solutes such as sugar molecules, and/or proteins that form adsorption or depletion layers on the two leaflets of the bilayer membranes (Lipowsky and Döbereiner, 1998; Lipowsky, 2013; Rozycki and Lipowsky, 2015, 2016; Liu et al., 2016; Karimi et al., 2018; Ghosh et al., in preparation). Examples for mechanisms of local generation of membrane curvature are given in Box 5.1. Local curvature generation by proteins is reviewed in Chapter 23 of this book.

Box 5.1 Local generation of membrane curvature

Bilayer asymmetry and spontaneous curvature can be generated by a variety of molecular mechanisms as illustrated in this Box.

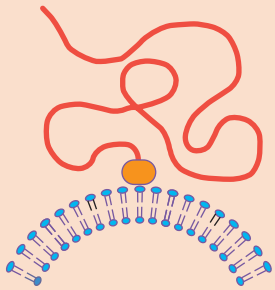

- A simple example is provided by a flexible polymer that is anchored with one of its ends to the membrane (Lipowsky, 1995; Nikolov et al., 2007).
- Such an anchored polymer generates curvature in order to increase its configurational entropy.

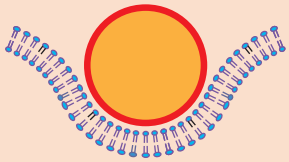

- Adhesive nanoparticles that are partially engulfed by the membrane act as scaffolds and impose their curvature onto this membrane, (Lipowsky and Döbereiner, 1998; Deserno, 2004; Agudo-Canalejo and Lipowsky, 2015a) see Chapter 8 of this book.

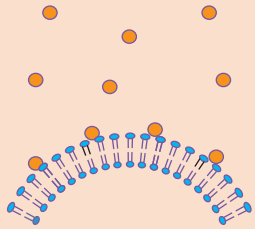

- Small adhesive solutes generate a substantial spontaneous curvature m as predicted theoretically (Lipowsky and Döbereiner, 1998; Lipowsky, 2013) and observed in molecular simulations (Rozycki and Lipowsky, 2015). For particles with a diameter of 1 nm and a concentration difference of 100 mM, adsorption leads to $m = \frac{1}{77nm}$.

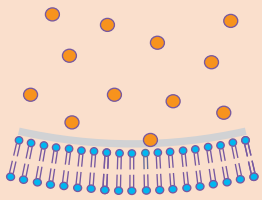

- Depletion layers of solutes induce a spontaneous curvature m of the opposite sign (Lipowsky and Döbereiner, 1998). This prediction has also been confirmed by recent molecular simulations (Rózycki and Lipowsky, 2016). For particles with a diameter of 1 nm and a concentration difference of 100 mM, depletion leads to $m = -\frac{1}{270nm}$.

The case of divalent ions is controversial because two recent experimental studies on Ca^{2+} ions (Simunovic et al., 2015; Baumgart et al., 2017) led to different conclusions about the sign of the ion-induced spontaneous curvature.

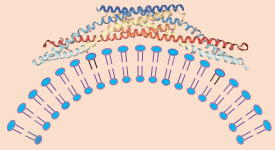

- N-BAR proteins such as amphiphysin (Takei et al., 1999; Peter et al., 2004) and endophilin (Farsad et al., 2001), F-BAR proteins such as pacsin/syndapin (Wang et al., 2009), and other proteins involved in endocytosis such as epsin (Ford et al., 2002) can bind to membranes and impose their curvature onto these membranes.

Membrane-binding proteins that act as scaffolds for the membrane shape are usually quite rigid. They can be regarded as adhesive nanoparticles with two characteristic properties: (i) their shape is typically nonspherical and often banana-like or convex-concave; and (ii) their surface contains a more or less complex pattern of adhesive and nonadhesive surface domains. Thus membrane-binding proteins that impose their shape onto the membrane can be regarded as nonspherical Janus-like nanoparticles.

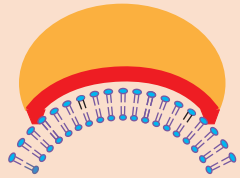

- If the *planar* membrane can bind to some of the adhesive surface domains (red) of the particle, the particle generates membrane curvature via an induced-fit mechanism.

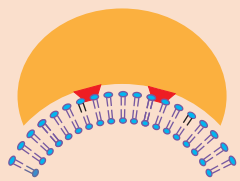

- If the adhesive surface domains (red) can only be reached by an appropriately *curved* membrane, the particle generates membrane curvature via conformational selection (Lipowsky, 2014b).

On length scales that exceed about twice the membrane thickness, the bilayer asymmetry can be described in terms of another curvature-elastic parameter, the spontaneous curvature m. In order to define the sign of m in an unambiguous manner, we use the same sign convention as for the mean curvature M, see Figure 5.9. Thus, we distinguish an interior from an exterior aqueous compartment and take the spontaneous curvature to be positive and negative if the membrane prefers to bulge towards the exterior and interior compartment, respectively. Note that, under the reversal of the normal vectors, the spontaneous curvature transforms in the same way as the mean curvature and, thus, changes sign.

If the membrane is decorated by many bound "particles," it will acquire a certain spontaneous curvature that depends both on the local particle-induced curvature and on the particle coverages for the two leaflets of the bilayer membrane (Breidenich et al., 2000; Lipowsky, 2002). Thus, if a single particle that is bound to the outer leaflet of an asymptotically flat bilayer generates the local, position-dependent mean curvature $M_{si}(s^1, s^2)$, the spontaneous curvature m is given by

$$m = I_{M,si}(\Gamma_{ex} - \Gamma_{in}) \tag{5.3}$$

with the integrated mean curvature

$$I_{M,si} \equiv \int dA M_{si}(s^1, s^2) \tag{5.4}$$

and the coverages Γ_{ex} and Γ_{in} which are equal to the numbers of particles bound to the outer and inner leaflets per unit area (Breidenich et al., 2000). In contrast to other elastic membrane parameters such as the bending rigidity or the area compressibility modulus, the spontaneous curvature can vary over more than three orders of magnitude, from the inverse size of giant vesicles, which is of the order of 1/(50 μm), to half the inverse membrane thickness, which is of the order of 1/(10 nm).

Inspection of the relationship Eq. 5.3 shows that the sign of the spontaneous curvature m is determined (i) by the sign of the integrated mean curvature $I_{M,si}$ induced by a single particle bound to the outer leaflet of the bilayer and (ii) by the sign of the difference $\Gamma_{ex} - \Gamma_{in}$ between the coverages of the outer and inner leaflets. Depending on the molar particle concentrations in the exterior and interior aqueous compartments, the sign of $\Gamma_{ex} - \Gamma_{in}$ can be positive or negative. Likewise, the sign of the integrated curvature $I_{M,si}$ can be positive or negative as well, reflecting different molecular interactions between the bound particle and the membrane. An anchored polymer, for example, generates a positive value of $I_{M,si}$ but this value becomes negative when all monomers of the polymer are strongly adsorbed onto the membrane (Breidenich et al., 2001, 2005). A negative sign of $I_{M,si}$ also applies if the particle is large and partially engulfed by the membrane.

As explained previously, we use two related conventions in order to define the sign of the local mean curvature of the membrane in an unambiguous manner. The first convention is that the normal vector of the membrane is taken to point towards the exterior compartment. The second convention is that we take the local mean curvature of the membrane to be positive if the membrane bulges in the direction of the normal vector. Therefore, the spontaneous curvature is taken to be positive as well if the membrane prefers to bulge towards the exterior solution, i.e., in the direction of the normal vector.

The intuitive notion that asymmetric membranes have a preferred curvature was originally discussed by Bancroft for surfactant monolayers in water-oil emulsions (Bancroft, 1913; Bancroft and Tucker, 1927) and was included by Frank as the so-called "splay term" in the curvature elasticity of liquid crystals (Frank, 1958). In the context of lipid bilayers, spontaneous curvature was first considered by Helfrich (1973), who introduced it in analogy to the splay term for liquid crystals. The corresponding curvature energy of the membrane is now known as the spontaneous curvature model (Seifert et al., 1991) which will be presented in the next section.

5.4 CURVATURE ELASTICITY OF UNIFORM MEMBRANES

This chapter describes the theoretical framework that has been crucial in order to understand the morphology of giant vesicles. This framework is based on membrane curvature and the associated elastic energy contributions. The theory also takes into account that the low lipid solubility and the osmotic conditions lead to important constraints on the membrane area and the vesicle volume. In fact, what makes this theory both appealing and challenging is the interplay between local and global membrane properties.

On the one hand, the shape of a membrane can be described locally by its mean and Gaussian curvatures. On the other hand, in the absence of topological transformations such as membrane fusion and fission, both the membrane area and the vesicle volume are essentially fixed which has a direct and strong influence on the local membrane behavior. The connection between local and global properties is provided by two quantities, the mechanical tension Σ within the membrane and the pressure difference ΔP across this membrane. For free vesicles, these two quantities cannot be measured experimentally. However, the theory described in this chapter provides explicit relations between Σ and ΔP and those quantities that are directly accessible to experimental observations.

Another intriguing aspect of the morphology of giant vesicles is the frequent observation of membrane necks that connect two larger membrane segments. One example is provided by the neck that connects the spherical bud to the mother vesicle in Figure 5.2, another example is provided by the shape L^{sto} in Figure 5.6. Theoretically, these necks were first discovered by numerical energy minimization (Seifert et al., 1991; Miao et al., 1991; Berndl et al., 1990) of vesicles with uniform membranes as considered in this section. The necks are interesting from a conceptual point of view because they lead to *local* relations between (i) geometric quantities that can be directly observed in the optical microscope and (ii) curvature-elastic parameters such as the spontaneous curvature.

This section focuses on the spontaneous curvature model which is theoretically appealing because it depends on a relatively small number of parameters. Indeed, uniform vesicle membranes involve two geometric quantities, the vesicle volume

V and the membrane area A, as well as two material parameters, the bending rigidity κ and the spontaneous curvature m introduced in Section 5.3.5. In fact, as shown below, the vesicle shapes depend only on two dimensionless parameters, the volume-to-area ratio proportional to $V/A^{3/2}$, also known as the reduced volume, and the dimensionless spontaneous curvature proportional to $mA^{1/2}$.

The spontaneous curvature model is based on an expansion in powers of the principal curvatures and should be reliable as long as these curvatures are small compared to the inverse membrane thickness. In addition, the spontaneous curvature model implicitly assumes that the area difference between the two leaflets can change via flip-flops of lipid molecules. While a phospholipid molecule may stay in the same leaflet for hours, a cholesterol molecule will, on average, flip-flop from one leaflet to the other within one second. Therefore, the spontaneous curvature model should provide a reliable description for bilayer membranes that contain cholesterol or another sterol. The latter membranes are of particular interest because they undergo phase separation into liquid-disordered and liquid-ordered phases, see Section 5.8 below and Chapter 18 of this book.

If all membrane components undergo relatively slow flip-flops, one should extend the spontaneous curvature model by adding a nonlocal term that depends on the quenched area difference between the two leaflets. This extension leads to the area-difference-elasticity model and to an effective spontaneous curvature as described at the end of this section.

The present section is supplemented by three appendices: Appendix 5.B on different topologies of vesicles; Appendix 5.D which explains the identity of the mechanical tension with the Lagrange multiplier for membrane area; and Appendix 5.E which describes the different variants of curvature models.

5.4.1 SPONTANEOUS CURVATURE MODEL

Curvature expansion of local curvature energy

Within the spontaneous curvature model, the curvature energy functional $\mathcal{E}_{\rm cu}\{S\}$ of a certain membrane shape S is provided by the area integral[4]

$$\mathcal{E}_{\rm cu}\{S\} = \int {\rm d}A\, \varepsilon_{\rm cu}(\underline{s}) \tag{5.5}$$

where $\varepsilon_{\rm cu}(\underline{s})$ represents a local energy density that varies smoothly with the two-dimensional surface coordinates $\underline{s} \equiv (s^1, s^2)$ used to parametrize the membrane surface via the three-dimensional vector $\vec{X}(\underline{s})$. When expressed in terms of these coordinates, the area element ${\rm d}A$ depends on the metric tensor g_{ij}, see Appendix 5.A , and has the form

$${\rm d}A = {\rm d}s^1 {\rm d}s^2 \sqrt{g} \quad \text{with} \quad g \equiv \det(g_{ij}) = g_{11}g_{22} - g_{12}g_{21}. \tag{5.6}$$

The local density $\varepsilon_{\rm cu}$ of the curvature energy should only depend on the principal curvatures C_1 and C_2. In addition, at any given point P of the membrane surface, this energy density must remain unchanged when we rotate the surface coordinates by $\pi/2$ which implies $\varepsilon_{\rm cu}(C_2, C_1) = \varepsilon_{\rm cu}(C_1, C_2)$. An expansion of $\varepsilon_{\rm cu}$ up to second order in the principal curvatures then leads to[5]

$$\varepsilon_{\rm cu}(C_1, C_2) \approx a_0 + a_1(C_1 + C_2) + a_2(C_1^2 + C_2^2) + a_3 C_1 C_2. \tag{5.7}$$

When this relation is expressed in terms of the mean curvature M and the Gaussian curvature G, we obtain

$$\varepsilon_{\rm cu} \approx 2\kappa(M - m)^2 + \kappa_G G \tag{5.8}$$

with the bending rigidity κ, the spontaneous curvature m, and the Gaussian curvature modulus κ_G.[6] As a result, the curvature energy functional has the form (Helfrich, 1973; Seifert et al., 1991)

$$\mathcal{E}_{\rm cu}\{S\} = \int {\rm d}A [2\kappa(M(\underline{s}) - m)^2 + \kappa_G G(\underline{s})] \tag{5.9}$$

which defines the spontaneous curvature model.

Vesicles without bilayer edges or pores

For a closed vesicle without bilayers edges or pores, the Gauss-Bonnet theorem of differential geometry implies

$$\int {\rm d}A G = 2\pi\chi = 2\pi(2 - 2\mathfrak{g}) \tag{5.10}$$

with the Euler characteristic χ and the topological genus $\mathfrak{g}$, which counts the number of handles, see Appendix 5.B. Thus, for a closed vesicle shape S and a uniform vesicle membrane, the spontaneous curvature model is defined by the curvature energy functional

$$\mathcal{E}_{\rm cu}\{S\} = \mathcal{E}_{\rm be}\{S\} + 2\pi\chi\kappa_G \tag{5.11}$$

with the bending energy functional

$$\mathcal{E}_{\rm be}\{S\} = 2\kappa \int {\rm d}A\, (M - m)^2. \tag{5.12}$$

When we evaluate the functionals $\mathcal{E}_{\rm cu}$ and $\mathcal{E}_{\rm be}$ for a certain shape S_o, we obtain the corresponding curvature and bending energies $E_{\rm cu} = \mathcal{E}_{\rm cu}\{S_o\}$ and $E_{\rm be} = \mathcal{E}_{\rm be}\{S_o\}$ for which we use normal capital letters E.

It is instructive to consider the behavior of the bending energy functional Eq. 5.12 under the reversal of the normal vectors. Thus, consider a certain shape S_o and map it onto another shape S_o' by reversing all normal vectors of its membrane surface. The mean curvature M of shape S_o is then transformed into the mean curvature $M'(\underline{s}) = -M(\underline{s})$ of shape S_o' which implies

[4] Here and below, large calligraphic letters such as $\mathcal{E}$ and $\mathcal{F}$ are used for functionals that map shapes into real numbers.

[5] Here and below, the symbol $\approx$ stands for 'asympotically equal' in a certain limit

[6] The constant term $a_0 - a_1^2/(4a_2)$ has been omitted.

$$\mathcal{E}_{\rm be}(\{S_o'\}, m') = \mathcal{E}_{\rm be}(\{S_o\}, m) \quad \text{for} \quad m' = -m, \tag{5.13}$$

i.e., the bending energy functional is invariant under a reversal of the normal vectors provided we reverse the spontaneous curvature m as well.

The bending energy functional $\mathcal{E}_{\rm be}\{S\} \sim \int {\rm d}A M^2$ of symmetric membranes with $m = 0$ has a long history in the calculus of variations. The quadratic expression in the mean curvature was first studied at the beginning of the 19th century by the French mathematician Germain in her theory of vibrating plates (Dalmédico, 1991). About a hundred years later, this expression played a prominent role in the work of the German mathematician Blaschke and his students, who were particularly interested in its invariance properties under conformal transformations. In the 1960s, the subject was studied in a systematic manner by the British mathematician Willmore, and the shapes that minimize $\int {\rm d}A M^2$ are often referred to as Willmore surfaces (Willmore, 1982).

Separation of length scales

As described above, the spontaneous curvature model is based on the expansion of the curvature energy density in powers of the principal curvatures and includes all terms up to second order in these curvatures. This truncation of the curvature expansion at second order is clearly appropriate as long as the principal curvatures are much smaller than the inverse membrane thickness $1/\ell_{\rm me} \simeq 1/(4\ {\rm nm})$ as follows from the discussion in Section 5.3.1. Thus, the spontaneous curvature model should provide a reliable description for the shapes of giant vesicles as observed in the (conventional) optical microscope, which resolves membrane curvatures below 1/(300 nm). In fact, as explained in Appendix 5.C.1, the spontaneous curvature model is expected to be quite reliable up to principal curvatures of about 1/(80 nm). For more strongly curved membrane segments, third-order curvature terms may become important which involve two additional curvature-elastic parameters, see Appendix 5.C.1.

5.4.2 SPONTANEOUS TENSION

The bending energy functional as given by Eq. 5.12 attains its minimal value, $\mathcal{E}_{\rm be} = 0$, when we consider shapes for which the mean curvature M is equal to the spontaneous curvature m. The expression Eq. 5.12 also implies that the bending rigidity κ represents a "spring constant" for deviations of the actual mean curvature M from the spontaneous curvature m of the membrane.

Real membranes experience a variety of constraints that necessarily lead to such deviations of M from m. One important constraint is provided by the size of the membrane. If the membrane area A is large compared to $4\pi/m^2$, which is the surface area of a sphere with radius $1/|m|$, the membrane cannot adapt its curvature to the spontaneous curvature by forming a single sphere but can do so, to a large extent, by forming a long cylinder with radius $R_{\rm cy} = 1/(2m)$. Another important constraint arises from the osmotic conditions that determine the vesicle volume and, thus, the volume-to-area ratio, also known as the reduced volume. If the vesicle volume is increased by osmotic inflation, it will eventually attain a spherical shape with mean curvature $M = 1/R_{\rm sp}$ that usually differs from the spontaneous curvature m of the vesicle membrane. In fact, for a giant spherical vesicle, the mean curvature $M = 1/R_{\rm sp}$ can be very small compared to the absolute value $|m|$ of the spontaneous curvature. Likewise, supported lipid bilayers with $M = 0$ can have a large spontaneous curvature with magnitude $|m| \gg 0$. Whenever a large membrane segment of area A is forced to attain a mean curvature that is much smaller than the spontaneous curvature, the contribution of this segment to the bending energy obtained from Eq. 5.12 has the form $E_{\rm be} \approx A\sigma$ with the spontaneous tension (Lipowsky, 2013)

$$\sigma \equiv 2\kappa m^2. \tag{5.14}$$

This tension represents the only tension scale that can be defined, apart from a dimensionless multiplicative factor, by the two parameters κ and m. Therefore, the spontaneous tension σ may be viewed as the intrinsic tension of curvature elasticity. If the membrane has a bending rigidity of about 10^{-19} J, a spontaneous curvature of 1/(20 μm) leads to a spontaneous tension of about 10^{-6} mN/m while a spontaneous curvature of 1/(20 nm) leads to a spontaneous tension of about 1 mN/m. Thus, in real membrane systems, the spontaneous tension can vary over six orders of magnitude, see the examples in Table 5.1.

5.4.3 GLOBAL AND LOCAL PARAMETERS

Volume and area as global control parameters

As explained in Section 5.2.2, lipid bilayers are permeable to water and small gas molecules but essentially impermeable to ions and solute molecules, see also Chapter 20 of this book. As a consequence, the vesicle volume is primarily determined

Table 5.1 Spontaneous (or preferred) curvature m in units of 1/μm and associated spontaneous tension $\sigma = 2\kappa m^2$ in units of 2 mN/m for four different membrane systems where the bending rigidity was taken to have the typical value $\kappa \simeq 10^{-19}$ J.

	SUGAR SOLUTIONS[a]	DNA STRANDS[b]	PEG/DEXTRAN SOLUTIONS[c]	BAR-DOMAIN PROTEINS[d]
m [1/μm]	0.01–0.1	0.1–1	3–10	10–50
σ [2 mN/m]	10^{-8}–10^{-6}	10^{-6}–10^{-4}	10^{-3}–10^{-2}	10^{-2}–0.5

[a] Döbereiner, H.G. et al., *Eur. Biophys. J.*, 28, 174–178, 1999.
[b] Nikolov, V. et al., *Biophys. J.*, 92, 4356–4368, 2007.
[c] Li, Y. et al., *Proc. Nat. Acad, Sci. USA*, 108, 4731–4736, 2011; Liu, Y. et al., *ACS Nano*, 10, 463–474, 2016.
[d] Peter, B.J. et al., *Science*, 303, 495–499, 2004; McMahon, H.T. and Gallop, J.L. *Nature*, 438, 590–596, 2005.

by the osmotic conditions and the temperature. Therefore, one convenient procedure to change the vesicle volume at constant temperature is via osmotic inflation and deflation. Osmotic deflation is limited by the attractive intermolecular forces that start to become important when different membrane segments come into close proximity. Thus, at very small volumes, different segments of the vesicle membrane may start to fold back onto themselves or to form local membrane stacks. On the other hand, osmotic inflation is limited by the available membrane area. Indeed, for a given membrane area A and the corresponding vesicle size

$$R_{\rm ve} = \sqrt{A/(4\pi)}, \tag{5.15}$$

the vesicle volume V attains its maximal value when the vesicle has a spherical shape. Therefore, the vesicle volume satisfies the inequality

$$V \le \frac{4\pi}{3} R_{\rm ve}^3 = \frac{4\pi}{3}\left(\frac{A}{4\pi}\right)^{3/2}. \tag{5.16}$$

For constant temperature and lipid composition, the area A of the vesicle membrane is primarily determined by the number of lipid molecules within the membrane. Indeed, in the absence of external forces or constraints, the lipids attain a certain molecular area corresponding to their optimal packing density. In principle, the membrane area can be changed by a mechanical tension that acts to stretch the membrane. In practice, such a tension can increase the membrane area only by a few percent because the membrane starts to rupture for larger extensions of its area. Therefore, as long as the membrane does not rupture, the membrane area A should attain a constant value to a very good approximation.

For giant unilamellar vesicles, one can directly measure the vesicle volume V and the membrane area A. It is therefore rather natural from an experimental point of view to regard V and A as basic geometric parameters that determine the vesicle shape.

Dimensionless parameters of spontaneous curvature model

For closed vesicles, the Gaussian curvature modulus contributes a constant term to the curvature energy functional $\mathcal{E}_{\rm cu}$ which is independent of the vesicle shape. We are then left with the bending energy functional $\mathcal{E}_{\rm be}$ that depends on four (dimensionful) parameters: two material parameters, namely bending rigidity κ and spontaneous curvature m, as well as two geometric parameters, vesicle volume V and membrane area A. Furthermore, we can choose a basic energy and length scale. One convenient choice for these two scales is provided by the bending energy κ and the vesicle size $R_{\rm ve}$ as defined by Eq. 5.15.

For the latter choice, the dimensionless bending energy $E_{\rm be}/\kappa$ depends only on two dimensionless parameters: (i) the volume-to-area ratio or reduced volume of the vesicle

$$v \equiv \frac{V}{\frac{4\pi}{3} R_{\rm ve}^3} = 6\sqrt{\pi}\, V/A^{3/2} \tag{5.17}$$

and (ii) the rescaled and dimensionless spontaneous curvature

$$\bar{m} \equiv m R_{\rm ve} = m\sqrt{A/(4\pi)}. \tag{5.18}$$

In the following, we will often discuss the behavior of vesicles with a certain, fixed membrane area and, thus, with a fixed length scale $R_{\rm ve}$. Deflation and inflation processes are then described by changes in the volume v for a certain value of the spontaneous curvature $\bar{m}$. Likewise, adsorption and desorption processes which affect the bilayer asymmetry are described by changes of the spontaneous curvature $\bar{m}$ for a fixed value of the volume v.

Scale transformations of vesicle shapes

The conclusions of the previous subsection can be understood from a somewhat different perspective if we study the behavior of the energy functional in Eq. 5.12 under scale transformations. As mentioned, the vesicle shape S can be described by a vector-valued function $\vec{X}(\underline{s})$ that depends on the two-dimensional surface coordinate $\underline{s}$. A scale transformation from the shape S to the new shape S' is then described by

$$\vec{X}(\underline{s}) \to \vec{X}'(\underline{s}) \equiv \zeta\, \vec{X}(\underline{s}) \quad \text{with a scale factor } \zeta > 0 \tag{5.19}$$

which implies the scale transformations

$$V \to V' = \zeta^3 V \quad \text{and} \quad A \to A' = \zeta^2 A \tag{5.20}$$

of vesicle volume and membrane area.

The bending energy functional $\mathcal{E}_{\rm be}$ in Eq. 5.12 remains invariant under the scale transformation Eq. 5.19, i.e., $\mathcal{E}_{\rm be}\{S'\} = \mathcal{E}_{\rm be}\{S\}$ if we combine this transformation with the rescaling

$$m \to m' \equiv m/\zeta \tag{5.21}$$

of the spontaneous curvature.

Now, assume that we have minimized the energy functional and found the shape S_0 of minimal bending energy for a certain set of the (dimensionful) parameters V, A, κ, and m. Any slightly deformed shape, say S_1, will have a larger bending energy, i.e., $\mathcal{E}_{\rm be}\{S_1\} > \mathcal{E}_{\rm be}\{S_0\}$. This property remains valid if we compare the bending energies of the shapes S_0' and S_1' as obtained by rescaling both S_0 and S_1 with the same scale factor ζ, i.e., $\mathcal{E}_{\rm be}\{S_1'\} > \mathcal{E}_{\rm be}\{S_0'\}$ for any small deformation of S_0', provided we also rescale the spontaneous curvature according to Eq. 5.21. Therefore, the rescaled shape S_0' represents the shape of minimal bending energy for the parameters $\zeta^3 V$, $\zeta^2 A$, κ, and m/ζ.

The same conclusion can be drawn from the dimensionless parameters introduced in the previous subsection. Indeed, the dimensionless bending energy $E_{\rm be}/\kappa$ depends only (i) on the volume-to-area ratio $v \propto V/A^{3/2}$ and (ii) on the spontaneous curvature $\bar{m} = mR_{\rm ve}$, both of which remain invariant under the combined scale transformation Eqs 5.20 and 5.21.

It is often instructive to consider the special case of a symmetric membrane with vanishing spontaneous curvature, $m = 0$. In this case, the energy functional Eq. 5.12 is invariant under

the scale transformation of the vesicle geometry as described by Eq 5.20 and does not involve the rescaling of any material parameter. Thus, for $m = 0$, large and small vesicles have the same bending energy if they have the same shape.

5.4.4 LOCAL SHAPE EQUATION AND ENERGY BRANCHES

Constrained energy minimization

If we take the vesicle volume and the membrane area as control parameters, we are thus faced with the problem of minimizing the curvature energy functional as given by Eq. 5.11 for a given vesicle volume V and membrane area A. In principle, there are a variety of ways to tackle this minimization problem numerically.

Numerical minimization typically involves a discretization of the vesicle shape into a triangular mesh of membrane patches. Furthermore, in order to model the fluidity of the membrane, one has to choose a dynamic triangulation. The advantage of numerical minimization is that we do not have to make any simplifying assumptions about the vesicle shape. The disadvantage of such a numerical procedure is that we can only explore a limited region of the parameter space. Furthermore, numerical minimization methods becomes difficult whenever the vesicle shape involves narrow membrane necks or long tubes. As we will see further below, such somewhat exotic shapes are quite common for vesicle membranes.

In order to apply analytical approaches to the constrained minimization, we will now incorporate the area and volume constraints via Lagrange multipliers Σ and ΔP and consider the shape functional

$$\mathcal{F}\{S\} = -\Delta P \mathcal{V}\{S\} + \Sigma \mathcal{A}\{S\} + \mathcal{E}_{\rm be}\{S\} \tag{5.22}$$

where we have omitted the shape-independent term arising from the integrated Gaussian curvature. The two Lagrange multipliers have to be chosen in such a way that the volume functional $\mathcal{V}$ and the area functional $\mathcal{A}$ attain the values $\mathcal{V}\{S\} = V$ and $\mathcal{A}\{S\} = A$. Note that we again denote the functionals $\mathcal{F}$, $\mathcal{V}$, and $\mathcal{A}$ by large calligraphic letters and their numerical values for a certain shape by normal capital letters F, V, and A.

As shown in Appendix 5.D, the Lagrange multiplier Σ can be identified with the mechanical tension experienced by the uniform membrane. The latter identity can be derived by defining the overall elastic energy of the membrane to be the sum of its bending and stretching energy and by minimizing this overall elastic energy (Lipowsky, 2014a).

Euler-Lagrange or local shape equation

The first variation of the shape functional $\mathcal{F}\{S\}$ leads to the Euler-Lagrange equation

$$\Delta P = 2\Sigma M - 2\kappa \nabla^2_{\rm LB} M - 4\kappa [M - m][M(M + m) - G] \tag{5.23}$$

with the Laplace-Beltrami operator $\nabla^2_{\rm LB}$ and the (local) Gaussian curvature G. When expressed in terms of the surface coordinates $\underline{s}$, the action of this operator onto a scalar function $f(\underline{s})$ has the explicit form

$$\nabla^2_{\rm LB} f = \frac{1}{\sqrt{g}} \frac{\partial}{\partial s^k} \left(\sqrt{g}\, g^{kj} \frac{\partial}{\partial s^j} f \right) \tag{5.24}$$

with the inverse metric tensor $(g^{ij}) \equiv (g_{ij})^{-1}$ and an implicit summation over repeated indices (do Carmo, 1976). Note that the Euler-Lagrange Eq. 5.23 provides an explicit relation between the Lagrange multipliers ΔP and Σ with the mean and Gaussian curvatures, M and G, which describe the membrane shape locally. Therefore, the Euler-Lagrange equation represents a *local* shape equation.

The Euler-Lagrange Eq. 5.23 is equivalent to

$$\Delta P = 2\hat{\Sigma} M - 2\kappa \nabla^2_{\rm LB} M - 4\kappa m M^2 - 4\kappa [M - m][M^2 - G] \tag{5.25}$$

with the total membrane tension

$$\hat{\Sigma} \equiv \Sigma + 2\kappa m^2 = \Sigma + \sigma \tag{5.26}$$

which represents the sum of the mechanical tension Σ and the spontaneous tension σ, where we identified the Lagrange multiplier Σ with the mechanical tension, see Appendix 5.D. Therefore, the only tension that enters the solution of the Euler-Lagrange equation is the total tension $\hat{\Sigma}$ that contains the spontaneous tension σ defined in Eq. 5.14.

For spontaneous curvature $m = 0$, the Euler-Lagrange Eq 5.23 assumes the simplified form

$$\Delta P = 2\Sigma M - 2\kappa \nabla^2_{\rm LB} M - 4\kappa M [M^2 - G] \quad (m = 0) \tag{5.27}$$

which was derived by several mathematicians as reviewed in the monograph of Willmore (Willmore, 1982). It seems that the variation of the more general case with $m \neq 0$ was first considered by (Jenkins, 1977) who included both normal and tangential displacements of the membrane surface.[7] However, in order to derive the Euler-Lagrange Eq. 5.23, it is sufficient to include only normal displacements as shown by (Ou-Yang and Helfrich, 1989).

Energy branches of stationary shapes

The solutions of the Euler-Lagrange Eq. 5.23 represent the stationary shapes corresponding to local minima, saddle points, or local maxima of the bending energy. The physically relevant shapes are the local minima, which represent (meta)stable states, and the saddle points which provide the activation barriers between different (meta)stable states.

In practice, the combination of the Laplace-Beltrami operator and the nonlinearities in the principal curvatures C_1 and C_2, arising from the second and third power of the mean curvature $M = \frac{1}{2}(C_1 + C_2)$ and from the Gaussian curvature $G = C_1 C_2$, make the Euler-Lagrange Eq. 5.23 rather difficult to solve. As explained further below, much insight can be obtained for special shapes such as spheres, cylinders, and combinations

[7] The final result of the variational calculation by (Jenkins, 1977) contains one term that is cancelled by another, missing term.

thereof. For axisymmetric shapes, the partial differential Eq 5.23 is equivalent to a set of ordinary differential equations that can be solved numerically, e.g., by shooting methods. In this way, the regime of relatively small spontaneous curvatures m with $|\bar{m}| = |m| R_{ve} \lesssim 2$ has been studied in a systematic manner (Seifert et al., 1991).

These numerical solutions have shown that the stationary shapes form, in general, several branches for the same set of parameters as illustrated in Figure 5.12.[8] The latter figure displays the branches for vanishing spontaneous curvature $m = 0$. The different branches will now be labeled by the index j and the corresponding stationary shapes by S^j. Along branch j, the bending energy function

$$E_{be}(V, A; \kappa, m; j) = \mathcal{E}_{be}\{S^j\} \tag{5.28}$$

varies in a continuous manner as one changes one of the control parameters. When expressed in terms of the dimensionless parameters v and $\bar{m} = mR_{ve}$ as defined in Eqs 5.17 and 5.18, one obtains

$$E_{be}(V, A; \kappa, m; j) = 8\pi\kappa \bar{E}(v, \bar{m}; j), \tag{5.29}$$

see Figure 5.12. The corresponding shapes of minimal energy are displayed in Figure 5.13.

Pressure difference and membrane tension

In order to get further insight into the two Lagrange multipliers ΔP and Σ, it is useful to consider the shape energy

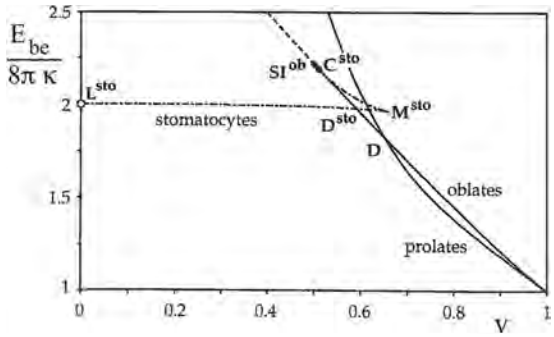

Figure 5.12 Dimensionless bending energy $\bar{E}_{be} = E_{be}/(8\pi\kappa)$ as a function of volume-to-area ratio v for spontaneous curvature $m = 0$: The sphere corresponds to the largest possible volume-to-area ratio $v = 1$. In the limit of small v, we obtain the limit shape L^{sto} of a stomatocyte consisting of two concentric spheres of (almost) equal size connected by a closed membrane neck. The two full lines emanating from the sphere correspond to (meta)stable prolates and oblates. The dashed-dotted line connecting the limit shape L^{sto} with the transition point D^{sto} corresponds to stable stomatocytes, the one between D^{sto} and M^{sto} to metastable stomatocytes, and the dashed-dotted line between M^{sto} and C^{sto} to the activation barriers between the oblates and the stomatocytes. (Reproduced from Seifert, U. et al., *Phys. Rev. A*, 44, 1182–1202, 1991.)

[8] The 'branches' are really two-dimensional sheets over the $(v, \bar{m})$-plane.

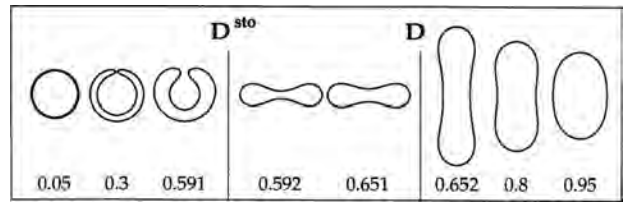

Figure 5.13 Axisymmetric shapes of a vesicle with constant area A and variable volume V as expressed in terms of the dimensionless volume v (bottom row) for spontaneous curvature $\bar{m} = 0$. (Reproduced from Seifert, U. et al., *Phys. Rev. A*, 44, 1182–1202, 1991.)

$$F(\Delta P, \Sigma; \kappa, m; j) \equiv -\Delta P V + \Sigma A + E_{be}(V, A; \kappa, m; j) \tag{5.30}$$

along a certain branch j of stationary shapes and to interpret this expression as the Legendre-transformed energy from the extensive variables V and A to the intensive variables ΔP and Σ. The formal structure of such a Legendre transformation, which plays an important role in thermodynamics, implies (Svetina and Zeks, 1989; Seifert et al., 1991; Miao et al., 1991; Seifert, 1997)

$$\Delta P = \left(\frac{dE_{be}(V, A; \kappa, m; j)}{dV} \right)_A \tag{5.31}$$

and

$$\Sigma = -\left(\frac{dE_{be}(V, A; \kappa, m; j)}{dA} \right)_V . \tag{5.32}$$

When we have several branches of stationary shapes for the same values of V and A, the derivatives on the right hand side of these relations will depend on the branch index j and so will the values of ΔP and Σ, compare Figure 5.12.

The relation Eq. 5.31 implies that the Lagrange multiplier ΔP is the pressure conjugate to the vesicle volume V and can, thus, be identified with the difference

$$\Delta P = P_{in} - P_{ex} \tag{5.33}$$

between the pressures P_{in} and P_{ex} within the interior and exterior compartments. In practise, these pressures are usually osmotic pressures but may also include hydrostatic pressures as imposed by a micropipette. The pressure difference ΔP is usually orders of magnitude smaller than the individual osmotic pressures P_{in} and P_{ex}. The relation Eq. 5.32 implies that the Lagrange multiplier Σ is the tension conjugate to the membrane area A. In fact, as previously mentioned, this tension can be identified with the mechanical tension experienced by the uniform membrane as shown in Appendix 5.D (Lipowsky, 2014a).

When expressed in terms of the dimensionless bending energy $\bar{E}_{be} = E_{be}/(8\pi\kappa)$, the general relations Eqs 5.31 and 5.32 for the pressure difference and the membrane tension can be rewritten in the form

$$\frac{\Delta P}{8\pi\kappa} = \left(\frac{dv}{dV} \right)_A \frac{\partial \bar{E}_{be}}{\partial v} = 6\sqrt{\pi} \frac{1}{A^{3/2}} \frac{\partial \bar{E}_{be}}{\partial v} \tag{5.34}$$

or

$$\frac{\Delta P R_{ve}^3}{\kappa} = 6\frac{\partial \bar{E}_{be}}{\partial v} \tag{5.35}$$

and

$$\frac{\Sigma}{8\pi\kappa} = 9\sqrt{\pi}\,\frac{V}{A^{5/2}}\frac{\partial \bar{E}_{be}}{\partial v} - \frac{1}{4\sqrt{\pi}}\,\frac{m}{A^{1/2}}\frac{\partial \bar{E}_{be}}{\partial \bar{m}} \tag{5.36}$$

or

$$\frac{\Sigma R_{ve}^2}{\kappa} = 3v\frac{\partial \bar{E}_{be}}{\partial v} - \bar{m}\frac{\partial \bar{E}_{be}}{\partial \bar{m}}. \tag{5.37}$$

For vanishing spontaneous curvature, $\bar{m} = m = 0$, the second term in Eqs 5.37 and 5.36 vanishes which implies that both ΔP and Σ become proportional to the partial derivative $\partial \bar{E}_{be}/\partial v$. Inspection of Figure 5.12 shows that this derivative is negative along the prolate and oblate branch but close to zero along the stomatocyte branch. Thus, as we reduce the volume of a spherical vesicle with $m = 0$, the pressure difference ΔP and the membrane tension Σ are both negative along the prolate and oblate branches. A negative pressure difference $\Delta P = P_{in} - P_{ex}$ implies that the exterior osmotic pressure exceeds the interior one and that the pressure difference acts to compress the vesicle volume. A negative tension Σ implies that the membrane is slightly compressed compared to its optimal packing density. Along the stomatocyte branch, on the other hand, both the pressure difference and the membrane tension are close to zero.

A combination of the two relations Eqs 5.34 and 5.36 leads to

$$3\Delta P V - 2\Sigma A = 4\sqrt{\pi}\,\frac{\kappa m}{A^{1/2}}\frac{\partial \bar{E}_{be}}{\partial \bar{m}}, \tag{5.38}$$

independent of the derivative $\partial \bar{E}_{be}/\partial v$ which cancels out from this special combination of ΔP and Σ. In the absence of a spontaneous curvature, we then obtain the simple relation

$$3\Delta P V = 2\Sigma A \quad (m = 0). \tag{5.39}$$

We will see in the next subsection that the same relation also follows from special deformations (or variations) of the stationary shapes as provided by infinitesimal scale transformations.

5.4.5 GLOBAL SHAPE EQUATION

Now, consider a certain stationary shape S^j of the shape functional $\mathcal{F}$ as given by Eq. 5.22. The pressure difference ΔP and the tension Σ then have specific values as obtained from the partial derivatives in Eqs 5.31 and 5.32 along the corresponding branch that includes the chosen shape S^j. Small deformations of this shape can be described by membrane displacements $\vec{u}(\underline{s})$ which define the deformed shape S' via

$$\vec{X}(\underline{s}) \to \vec{X}'(\underline{s}) = \vec{X}(\underline{s}) + \varepsilon\,\vec{u}(\underline{s}) \quad \text{with} \quad |\,\varepsilon\,| \ll 1. \tag{5.40}$$

Because the shape S^j represents a local minimum or saddle point of the shape functional F, we know that

$$\mathcal{F}\{S'\} - \mathcal{F}\{S^j\} = O(\varepsilon^2) \quad \text{or} \quad \frac{d\mathcal{F}\{S'\}}{d\varepsilon}|_{\varepsilon=0} = 0. \tag{5.41}$$

A particular shape deformation is provided by the choice $\vec{u}(\underline{s}) = \vec{X}(\underline{s})$ which leads to the infinitesimal scale transformation

$$\vec{X}(\underline{s}) \to \vec{X}'(\underline{s}) = (1+\varepsilon)\vec{X}(\underline{s}). \tag{5.42}$$

This scale transformation implies that the area A and the volume V are transformed according to $A \to A' = (1+\varepsilon)^2 A$ and $V \to V' = (1+\varepsilon)^3 V$. Likewise the integrated mean curvature

$$I_M = \mathcal{I}_M\{S\} \equiv \int \mathrm{d}A M \tag{5.43}$$

transforms according to

$$I_M = \mathcal{I}_M\{S\} \to I_M' = \mathcal{I}_M\{S'\} = (1+\varepsilon) I_M \tag{5.44}$$

while the integral $\int \mathrm{d}A M^2$ remains unchanged. When applied to the explicit form of the shape functional $\mathcal{F}$, the condition Eq 5.41 leads to

$$-3\Delta P V + 2\hat{\Sigma} A - 4\kappa m I_M = 0 \tag{5.45}$$

with the total membrane tension $\hat{\Sigma} = \Sigma + 2\kappa m^2$ as in Eq. 5.26. For any stationary shape S^j, this equation provides an explicit connection between ΔP, $\hat{\Sigma}$ and the global geometric quantities V, A, and I_M. Therefore, Eq. 5.45 represents a *global* shape equation.

For $m = 0$, the global shape equation reduces to the relation Eq. 5.39. Furthermore, a combination of Eq. 5.45 with Eq. 5.38 leads to the expression

$$\frac{\partial \bar{E}_{be}}{\partial \bar{m}} = 2\bar{m} - \frac{I_M}{\sqrt{\pi A}} \tag{5.46}$$

for the partial derivative of the dimensionless bending energy $\bar{E}_{be}(v, \bar{m})$ with respect to the spontaneous curvature $\bar{m} = mR_{ve}$. Note that the integrated mean curvature I_M depends on the stationary shape S^j and, thus, on the spontaneous curvature $\bar{m}$.

5.4.6 VESICLE SHAPES WITH MEMBRANE NECKS

The numerical solutions of the Euler-Lagrange equations for axisymmetric shapes revealed that these shapes develop narrow membrane necks in certain regions of the parameter space and that these shapes approach limit shapes with closed necks. These necks provide information about the spontaneous curvature m as will be explained in the following subsections, see also Box 5.2 for a summary of necks for vesicle membranes with laterally uniform composition.

Neck closure condition

Let us consider a branch of stationary shapes S^{st} that represent local minima of the bending energy and, thus, solutions of the Euler-Lagrange Eq. 5.23. These shapes are smooth in the sense

that the shape variable $\vec{X}(s)$ is twice differentiable with respect to the surface coordinates and that the mean curvature varies continuously along an arbitrary path on the membrane surface. For any point P on this surface and for any path through this point, we can thus define two mean curvature values, M_{P+} and M_{P-}, which represent the limiting values of the mean curvature as we approach the point P from the "left" and from the "right" along the chosen path. The continuous variation of M then implies that

$$M_P = \frac{1}{2}(M_{P+} + M_{P-}). \tag{5.47}$$

For a smooth surface, we could also use the more general expression $M_P = \zeta M_{P+} + (1-\zeta)M_{P-}$ with $0 \le \zeta \le 1$ corresponding to different weights for the left-sided and the right-sided limit. However, because the assignment of "left" and "right" is completely arbitrary, we want the expression to remain unchanged when we interchange "left" and "right," which implies $\zeta = 1/2$. We now interpret the expression Eq. 5.47 as an interpolation formula and extend it to closed necks, i.e., to points on the membrane surface at which the mean curvature develops a discontinuity. Thus, if the two membrane segments, 1 and 2, adjacent to the closed neck have the mean curvatures M_1 and M_2, we define the effective curvature of the closed neck by

$$M_{ne} \equiv \frac{1}{2}(M_1 + M_2). \tag{5.48}$$

This definition is analogous to the value $H(0) = \frac{1}{2}$ of the Heaviside step function $H(x)$ as obtained from smooth approximations for $H(x)$.

The numerical studies of membrane necks also showed that the neck closure makes no contributions to the bending energy. Because the energy density at the neck is given by

$$\varepsilon_{be}(M_{ne}) \equiv 2\kappa[M_{ne} - m]^2, \tag{5.49}$$

we conclude that the neck closes in such a way that

$$M_{ne} = \frac{1}{2}(M_1 + M_2) = m \quad \text{(neck closure)}. \tag{5.50}$$

It follows from this condition that the two membrane segments 1 and 2 have the same bending energy density, i.e., that

$$\varepsilon_{be}(M_1) = \varepsilon_{be}(M_2). \tag{5.51}$$

In fact, we could also start from the requirement that the bending energy density is continuous across the closed neck which leads to $M_1 - m = \pm(M_2 - m)$. For the root with the plus sign, we obtain the relation $M_1 = M_2$, i.e., a continuous variation of M and, thus, no neck but, for the root with the minus sign, we recover the neck closure condition Eq. 5.50.

The neck closure condition Eq. 5.50 has been confirmed for a large number of axisymmetric shapes as obtained by minimizing the bending energy numerically (Seifert et al., 1991). So far, necks between non-axisymmetric membrane segments have not been studied in a systematic manner but the continuity arguments given above also apply to such non-axisymmetric situations and then lead to the same closure condition.

Neck closure of membrane buds

It is instructive to apply the condition Eq. 5.50 to the neck closure of membrane buds as frequently observed in experiments. Two cases can be distinguished corresponding to in- and out-buds that point towards the interior and exterior compartment, respectively, see Figure 5.14.

First, consider spherical out-buds as shown in Figure 5.14a–c. For such a bud with radius R_2, the bud membrane adjacent to the neck has positive mean curvature $M_2 = 1/R_2$. The 1-segment on the other side of the neck must satisfy $M_1 \ge -M_2$ because the two membrane segments cannot intersect each other. Combining this geometric constraint with the neck closure condition Eq 5.50, we obtain the inequality

$$m = \frac{1}{2}(M_1 + M_2) \ge 0 \quad \text{(neck closure of out-bud)} \tag{5.52}$$

for the spontaneous curvature m. Thus, whenever we observe the neck closure of an out-bud, we can conclude that the spontaneous curvature must be positive or zero. Furthermore, for $m = 0$, neck closure of an out-bud implies $M_1 = -M_2$, i.e., the 1-segment partially engulfs the bud membrane in the vicinity of the neck. Therefore, for a 1-segment with mean curvature $M_1 > -M_2 = -1/R_2$, neck closure of an *out-bud* implies a *positive* spontaneous curvature.

Next, consider spherical in-buds as shown in Figure 5.14d–f. For a spherical in-bud with radius R_2, the bud membrane adjacent to the neck has negative mean curvature $M_2 = -1/R_2$. The 1-segment on the other side of the neck must satisfy $M_1 \le -M_2 = |M_2|$ because the two membrane segments should not intersect each other.

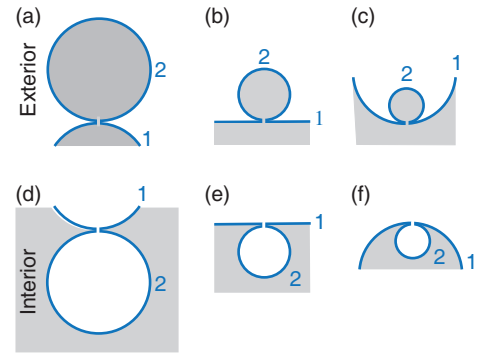

Figure 5.14 (a–c) Out-buds with closed necks, formed as limit shapes by a membrane with *positive* spontaneous curvature: The out-buds are filled with interior medium (gray) and point towards the exterior medium (white). The three membranes (blue) in (a–c) have the same spontaneous curvature $m > 0$ but differ in the mean curvatures of the 1- and 2-segments; (d–f) In-buds with closed necks, formed as limit shapes by a membrane with *negative* spontaneous curvature: The in-buds are filled with exterior medium (white) and point towards the interior medium (gray). The three membranes (blue) in (d–f) have the same spontaneous curvature $m < 0$ but differ in the mean curvatures of the two membrane segments. The two segments have mean curvature $M_1 = m$ and $M_2 = m$ in (a) and (d), $M_1 = 0$ and $M_2 = 2m$ in (b) and (e), and $M_1 = -m$ and $M_2 = 3m$ in (c) and (f).

A combination of the latter inequality with the neck closure condition Eq. 5.50 now leads to the condition

$$m = \frac{1}{2}(M_1 + M_2) \leq 0 \quad \text{(neck closure of in-bud)} \tag{5.53}$$

for the spontaneous curvature m. Thus, whenever we observe the neck closure of an in-bud, we can conclude that the spontaneous curvature must be negative or zero. For $m = 0$, neck closure of an in-bud now implies $M_1 = -M_2 = |M_2|$ as for the limit shape L^{sto} in Figure 5.12. Therefore, for a 1-segment with mean curvature $M_1 < |M_2| = 1/R_2$, neck closure of an *in-bud* implies a *negative* spontaneous curvature.

Stability of closed necks

The neck closure condition Eq. 5.50 applies to limit shapes as obtained from smooth solutions of the local shape Eq. 5.23 or the corresponding set of ordinary differential equations for axisymmetric shapes. One may also consider a closed neck and ask under what conditions this neck is locally stable. This problem has been addressed for axisymmetric vesicles consisting of two almost spherical vesicles that are connected by a narrow neck with radius R_{ne}. More precisely, these vesicle shapes consist of two spherical caps which are connected by two unduloid segments which form a membrane neck of radius R_{ne}. The shapes are parametrized in such a way that one can study the closure of the neck keeping the total membrane area constant. For vanishing neck radius R_{ne}, the shapes approach the two-sphere shapes Θ^{out} and Θ^{in}.[9] The two-sphere shape Θ^{out} consists of a sphere with radius R_1 and mean curvature $M_1 = 1/R_1$ connected, via a closed neck, to a spherical out-bud with radius $R_2 \leq R_1$ and mean curvature $M_2 = 1/R_2$ as in Figure 5.14a. The two-sphere shape Θ^{in} again consists of a sphere of radius R_1 and mean curvature $M_1 = 1/R_1$ but now connected, via a closed membrane neck, to a spherical in-bud with radius $R_2 \leq R_1$ and mean curvature $M_2 = -1/R_2$ as in Figure 5.14f. For small but nonzero R_{ne}, the bending energy of these vesicle shapes can then be expanded in powers of the neck radius R_{ne}.

If the two membrane segments 1 and 2 adjacent to the neck have positive mean curvatures as in Figure 5.14a, the bending energy is found to behave as (Fourcade et al., 1994)

$$E_{\text{be}}(R_{\text{ne}}) \approx E_{\text{be}}(0) - 4\pi\kappa(M_1 - m + M_2 - m)R_{\text{ne}} \quad \text{for small } R_{\text{ne}}. \tag{5.54}$$

On the other hand, if the 1-segment has positive mean curvature whereas the 2-segment has negative mean curvature as in Figure 5.14f, the bending energy has the asymptotic behavior (Lipowsky, 2014a)

$$E_{\text{be}}(R_{\text{ne}}) \approx E_{\text{be}}(0) + 4\pi\kappa(M_1 - m + M_2 - m)R_{\text{ne}} \quad \text{for small } R_{\text{ne}} \tag{5.55}$$

with a plus instead of a minus sign in front of the linear term. In both cases, the bending energy $E_{\text{be}}(0)$ of the two-sphere shapes Θ^{out} and Θ^{in}, which are characterized by vanishing neck radius $R_{\text{ne}} = 0$, does not involve any contribution from the neck itself.

The asymptotic behavior as given by Eq. 5.54 implies that the closed neck in Figure 5.14a, corresponding to an out-bud, is stable provided the average neck curvature M_{ne} satisfies

$$M_{\text{ne}} = \frac{1}{2}(M_1 + M_2) \leq m \quad \text{with } M_1 > 0 \text{ and } M_2 > 0 \tag{5.56}$$

but opens up if $M_{\text{ne}} > m$. The marginal case with $M_{\text{ne}} = m$ corresponds to the neck closure condition Eq. 5.52 with *positive* spontaneous curvature. Therefore, when a membrane with $m > 0$ forms a closed neck with $M_1 > 0$ and $M_2 > 0$ as in Figure 5.14a, this neck remains closed if the effective neck curvature M_{ne} decreases below the spontaneous curvature m.

On the other hand, the small R_{ne}-behavior in Eq. 5.55 implies that the closed neck of the in-bud in Figure 5.14f is stable provided

$$M_{\text{ne}} = \frac{1}{2}(M_1 + M_2) \geq m \quad \text{with } M_1 > 0 \text{ and } M_2 < 0 \tag{5.57}$$

but opens up if $M_{\text{ne}} < m$. Now, the marginal case with $M_{\text{ne}} = m$ corresponds to the neck closure condition Eq. 5.53 with *negative* spontaneous curvature. Therefore, when a membrane with $m < 0$ forms a closed neck with $M_1 > 0$ and $M_2 < 0$ as in Figure 5.14f, this neck remains stable if the effective neck curvature M_{ne} increases above the spontaneous curvature m, i.e., if the absolute value $|M_{\text{ne}}|$ of the effective neck curvature decreases below the absolute value $|m|$ of the spontaneous curvature.

The stability of a closed neck must not depend on our choice for the direction of the normal vectors. When we reverse the normal vectors, we change both the sign of the mean curvatures and the sign of the spontaneous curvature. Let us first apply this transformation to the neck configuration in Figure 5.14a which leads to the neck configuration in Figure 5.14d. The corresponding stability relation now becomes

$$M_{\text{ne}} = \frac{1}{2}(M_1 + M_2) \geq m \quad \text{with } M_1 < 0, M_2 < 0, \text{ and } m < 0. \tag{5.58}$$

Furthermore, if we reverse the normal vectors of the neck configuration in Figure 5.14f, we obtain the neck configuration in Figure 5.14c and the associated stability relation

$$M_{\text{ne}} = \frac{1}{2}(M_1 + M_2) \leq m \quad \text{with } M_1 < 0, M_2 > 0, \text{ and } m > 0. \tag{5.59}$$

In summary, we obtain essentially two different stability relations for the closed necks depicted in Figure 5.14. Closed necks with *non-negative* neck curvature M_{ne} can only exist for non-negative spontaneous curvature $m \geq 0$ and the neck curvature can then attain a value within the interval

$$0 \leq M_{\text{ne}} \leq m \quad \text{(out-bud, spontaneous curvature } m \geq 0) \tag{5.60}$$

[9] In the next Section 5.5 we will study such two-sphere vesicles in a systematic manner and distinguish limit shapes from persistent shapes. The two-sphere shapes Θ^{out} then correspond to the limit shapes L^{pea} and $L_{=}^{\text{out}}$ as well as to the persistent shapes Φ^{pea}. Likewise, the two-sphere shapes Θ^{in} represent both the limit shapes L^{sto} and $L_{=}^{\text{in}}$ as well as the persistent shapes Φ^{sto}.

which includes the neck configurations in Figure 5.14(a–c). The limiting case $M_{ne} = 0$ applies to an out-bud that is partially enclosed by the adjacent 1-segment of the mother vesicle whereas the equality $M_{ne} = m$ corresponds to the neck closure condition of the limit shape. An example for $M_{ne} = 0$ is provided by a discocyte with a membrane neck that connects the discocyte's north pole with mean curvature $M_1 < 0$ to a spherical out-bud with mean curvature $M_2 = -M_1 > 0$.

Closed necks with *non-positive* neck curvature M_{ne}, on the other hand, can only exist for non-positive spontaneous curvature $m \leq 0$ and the neck curvature can then have a value within the interval

$$0 \geq M_{ne} \geq m \quad \text{(in-bud, spontaneous curvature } m \leq 0) \tag{5.61}$$

which includes the neck configurations in Figure 5.14(d–f). Now, the neck closure condition $M_{ne} = m$ and the enclosed bud condition $M_{ne} = 0$ provide lower and upper bounds for the range of possible M_{ne}-values.

Mismatch between neck curvature and spontaneous curvature

For a stably closed neck that satisfies the inequalities $M_{ne} < m$ and $m < M_{ne}$ in Eqs 5.60 and 5.61, the bending energy density $\varepsilon_{be} = 2\kappa[M_{ne} - m]^2$ as given by Eq. 5.49 does not vanish. The closed neck may just be considered as a curvature "defect" as discussed in Appendix 5.C.2. In the continuum description used here, this defect is point-like and has vanishing area which implies that its bending energy vanishes as well. The latter property is explicitly borne out in the derivation of the relations Eqs 5.54 and 5.55 because the energies $E_{be}(0)$ obtained for vanishing neck radius $R_{ne} = 0$ do not contain any contribution from the neck.

However, a large mismatch between the neck curvature and the spontaneous curvature as obtained for stable necks with $0 < M_{ne} = m$ and $m = M_{ne} < 0$ does have an important consequence for the morphology of the vesicle. Indeed, a sufficiently large mismatch leads to an effective, curvature-induced constriction force that cleaves the membrane neck and thus leads to membrane fission, see Section 5.5.4 below.

5.4.7 AREA DIFFERENCE ELASTICITY

As mentioned at the beginning of this section, the spontaneous curvature model provides a quantitative description for the morphology of vesicles as long as the membrane curvatures are ~~large~~ compared to the inverse membrane thickness. Thus, highly curved membrane structures such as nanobuds or nanotubes may involve higher order curvature terms as discussed in ~~Appendix 5.E~~. In addition, the spontaneous curvature model implicitly assumes that the area difference between the two bilayer leaflets can change via fast flip-flops of at least one molecular membrane component. If flip-flops can be ignored on the experimentally relevant time scales, the spontaneous curvature model should be supplemented by an additional energy term as described in this subsection.

Nonlocal energy term for preferred area difference

The bending energy functional Eq. 5.12 represents the area integral over a *local* energy density. In general, the bending of a bilayer membrane consisting of two leaflets may be constrained in a *nonlocal* or *global* manner. Indeed, if the membrane molecules cannot undergo flip-flops between the two leaflets, the number of molecules are fixed within each leaflet and the quenched difference between these two numbers leads to a preferred area difference between these leaflets. This constraint was originally considered by Evans (1974), incorporated into the bilayer-coupling model by (Svetina and Zeks, 1989; Seifert et al., 1991), and generalized in terms of the area-difference-elasticity model (Miao et al., 1994; Döbereiner et al., 1997; Seifert, 1997).

The area difference ΔA between the area of the outer leaflet and the area of the inner leaflet is given by

$$\Delta A = 2 d_{mo} I_M \tag{5.62}$$

with the molecular length scale d_{mo}, which corresponds to the distance between the neutral surfaces of the two monolayers or leaflets, and the integrated mean curvature $I_M = \int \mathrm{d}A M$ as in Eq 5.43. The area-difference-elasticity model is defined by the energy functional

$$\mathcal{E}_{ADE}\{S\} = \mathcal{E}_{be}\{S\} + \mathcal{D}_{ADE}\{S\} \tag{5.63}$$

with the local energy functional $\mathcal{E}_{be}\{S\}$ as defined by Eq. 5.12 corresponding to the spontaneous curvature model and the nonlocal area-difference-elasticity term (Miao et al., 1994; Döbereiner et al., 1997)

$$\begin{aligned} \mathcal{D}_{ADE}\{S\} &= \frac{\pi\kappa_\Delta}{2Ad_{mo}^2}(\Delta\mathcal{A}\{S\} - \Delta A_0)^2 \\ &= \frac{2\pi\kappa_\Delta}{A}(\mathcal{I}_M\{S\} - I_{M,0})^2 \end{aligned} \tag{5.64}$$

where $\Delta\mathcal{A}\{S\}$ represents the area difference of the vesicle shape S and $\mathcal{I}_M\{S\}$ the integrated mean curvature of this shape. The additional energy term $\mathcal{D}_{ADE}$ introduces two new parameters, the second bending rigidity κ_Δ and the integrated mean curvature $I_{M,0} = \Delta A_0/2d_{mo}$, corresponding to optimal molecular areas in both leaflets (Seifert, 1997). These molecular areas are, however, not accessible to current experimental methods and depend on the mechanical membrane tension. If the leaflets of a large spherical vesicle with radius R_{ve} had optimal molecular areas, we would obtain

$$I_{M,0} = \int \mathrm{d}A \frac{1}{R_{ve}} = 4\pi R_{ve}. \tag{5.65}$$

Local and nonlocal spontaneous curvature

The stationary shapes with fixed membrane area A and fixed vesicle volume V are now more difficult to calculate because of the nonlocal character of the area-elasticity-difference but can be obtained using a two-step variational procedure, see Appendix 5.E. This procedure shows that all stationary shapes of the area-difference-elasticity model are also stationary shapes of the spontaneous curvature model with the shape functional $\mathcal{F}\{S\}$ as given by Eq. 5.22 and the effective spontaneous curvature (Döbereiner et al., 1997)

$$m_{eff} \equiv m + m_{nlo} \tag{5.66}$$

with the spontaneous curvature m, which is determined locally by the molecular interactions as considered in the previous subsections, and the nonlocal spontaneous curvature

$$m_{\rm nlo} \equiv \pi \frac{\kappa_\Delta}{\kappa} \frac{I_{M,0} - \mathcal{I}_M\{S^j\}}{A} \tag{5.67}$$

which depends on the stationary shape S^j via the integrated mean curvature $\mathcal{I}_M\{S^j\}$.

As mentioned before, area-difference-elasticity is only relevant if the membrane contains no molecular components that undergo flip-flops on the experimentally relevant time scales. Therefore, as far as the effective spontaneous curvature $m_{\rm eff}$ is concerned, we need to distinguish two cases: (i) For relatively fast flip-flops of some membrane components such as cholesterol, we can ignore the nonlocal spontaneous curvature $m_{\rm nlo}$ which implies that the effective spontaneous curvature $m_{\rm eff}$ becomes equal to the spontaneous curvature m, i.e., the area-difference-elasticity model reduces to the spontaneous curvature model; and (ii) For relatively slow flip-flops of all molecular membrane components, we will, in general, have a nonlocal spontaneous curvature $m_{\rm nlo}$ contributing to the effective spontaneous curvature $m_{\rm eff} = m + m_{\rm nlo}$. In order to examine whether this nonlocal spontaneous curvature $m_{\rm nlo}$ is relevant for a given vesicle shape, we need to determine its magnitude and to compare it with the local spontaneous curvature m.

Generalized stability relations for membrane necks

The latter approach can be applied, in particular, to two-sphere shapes with closed membrane necks. The stability of these necks can also be examined for the area-difference-elasticity model using the shape parametrization described in Section 5.4.6. Thus, we again consider axisymmetric shapes with membrane necks, parametrized in such a way that they approach the two-sphere shapes $\Theta^{\rm out}$ and $\Theta^{\rm in}$ in the limit of small neck radii. As before, the two-sphere shape $\Theta^{\rm out}$ consist of a sphere with a spherical out-bud and the two-sphere shape $\Theta^{\rm in}$ of a sphere with a spherical in-bud. We now use the energy functional Eq. 5.63 of the area-difference-elasticity model to calculate the elastic energy of the vesicle shapes up to first order in the neck radius $R_{\rm ne}$. One then finds that closed necks with positive curvature $M_{\rm ne}$ are stable if

$$0 < M_{\rm ne} \le m_{\rm eff} = m + \pi \frac{\kappa_\Delta}{\kappa} \frac{I_{M,0} - I_M\{\Theta^{\rm out}\}}{A} \tag{5.68}$$

(stable $\Theta^{\rm out}$ shapes)

and necks with negative curvature $M_{\rm ne}$ are stable if

$$0 \ge M_{\rm ne} \ge m_{\rm eff} = m + \pi \frac{\kappa_\Delta}{\kappa} \frac{I_{M,0} - \mathcal{I}_M\{\Theta^{\rm in}\}}{A} \tag{5.69}$$

(stable $\Theta^{\rm in}$ shapes).

These stability conditions involve three different types of quantities: (i) the neck curvature, a purely geometric quantity that can be directly deduced from the two-sphere shapes; (ii) the local spontaneous curvature m, a material parameter determined by the molecular interactions, and (iii) the non-local spontaneous curvature $m_{\rm nlo}$ that depends both on the geometry of the shape via the integrated mean curvature and on the bending rigidity ratio κ_Δ/κ. In subsection 5.5.3 further below, we will discuss the consequences of the stability conditions Eqs 5.68 and 5.69 for multi-sphere vesicles.

5.5 MULTI-SPHERE SHAPES OF UNIFORM MEMBRANES

In this section, we will consider a variety of multi-sphere shapes for vesicles with uniform membranes, i.e., membranes that have laterally uniform compositions and curvature-elastic properties. This section should be considered as a case study which nicely illustrates the polymorphism and multi-responsive behavior of giant vesicles.

We will focus on multi-component membranes that contain at least one membrane component such as cholesterol that undergoes relatively fast flip-flops. As mentioned, these membranes are appealing from a theoretical point of view because we can study their shapes within the spontaneous curvature model which depends only on two dimensionless parameters, the volume-to-area ratio (or reduced volume) v and the (local) spontaneous curvature $\bar{m}$. These two parameters can be controlled experimentally, e.g., by the osmotic conditions and by the adsorption of small solutes. In addition, three-component membranes with cholesterol have been of particular interest recently because they can form liquid-ordered and liquid-disordered phases. For both types of intramembrane phases, multi-sphere shapes have indeed been observed experimentally (Liu et al., 2016).

We will start with the Euler-Lagrange equations for spherical shapes which reveal the coexistence of two different sphere radii. When combined with the stability relations for the individual spheres and for the closed necks, we obtain multi-sphere vesicles that consist of several spheres with two different radii. We first consider two-sphere shapes and show that these shapes can be found in extended regions of the $(v, \bar{m})$-plane and that these regions are bounded by two types of limit shapes. We also examine the changes of the morphology diagram when area difference elasticity is taken into account. We conclude that these changes are negligible both for large spontaneous curvatures and for small bud sizes.

Multi-sphere shapes consisting of more than two spheres will also be discussed. One interesting example is provided by one sphere with radius R_1 and N spherical buds with radius R_2, all connected by closed necks that have the same neck curvature. For $N > 1$, the morphology diagram exhibits a more complex bifurcation structure with two bifurcation points and three types of limit shapes. The multi-sphere shapes with $N > 1$ buds described in this section are intimately related to the necklace-like tubes with $N > 1$ spherules as considered in the next Section 5.6.

5.5.1 SPHERICAL VESICLES AND SPHERICAL SEGMENTS

We now specify the local shape Eq. 5.23, which represents the Euler-Lagrange equation of the bending energy functional, and the global shape Eq. 5.45, which follows from the invariance of the bending energy under infinitesimal scale transformations,

to a spherical membrane segment with constant mean curvature $M = M_{sp}$. It turns out that *both shape equations lead to the same quadratic equation* for M_{sp} as given by

$$\Delta P = P_{in} - P_{ex} = 2\hat{\Sigma} M_{sp} - 4\kappa m M_{sp}^2 \tag{5.70}$$

with the total membrane tension $\hat{\Sigma} = \Sigma + \sigma$. For a symmetric bilayer membrane with $m = 0$, the relation Eq. 5.70 further simplifies and becomes

$$\Delta P = 2\Sigma M_{sp} \quad (m = 0) \tag{5.71}$$

which has the same form as the Laplace equation for liquid droplets. The Euler-Lagrange Eq. 5.70 can be derived in a more intuitive manner if one parametrizes the spherical shape by its radius R_{sp} and minimizes the shape energy with respect to R_{sp} (Lipowsky, 2013).

It follows from Eqs 5.70 and 5.71 that each value of $M_{sp} = \pm 1/R_{sp}$ defines a straight M_{sp}-line in the $(\Sigma,\Delta P)$-plane. For $m = 0$, these M_{sp}-lines cover the whole $(\Sigma,\Delta P)$-plane. For $m \neq 0$, on the other hand, the straight M-lines do not cover the whole $(\hat{\Sigma},\Delta P)$-plane as follows from the solution of the quadratic Eq. 5.70 which has the form

$$M_{1/2} = \frac{\hat{\Sigma}}{4\kappa m} \pm \left[\left(\frac{\hat{\Sigma}}{4\kappa m} \right)^2 - \frac{\Delta P}{4\kappa m} \right]^{1/2}. \tag{5.72}$$

Because the mean curvature must be real-valued, spherical segments are not possible for those values of $\hat{\Sigma}$ and ΔP for which the expression under the square root (or discriminant) becomes negative. Therefore, a certain choice of $\hat{\Sigma}$ and ΔP leads to spherical segments if

$$\Delta P \geq -\frac{\hat{\Sigma}^2}{4\kappa |m|} \quad \text{for} \quad m < 0 \tag{5.73}$$

and if

$$\Delta P \leq \frac{\hat{\Sigma}^2}{4\kappa m} \quad \text{for} \quad m > 0. \tag{5.74}$$

Along the parabolic boundaries $\Delta P = \hat{\Sigma}^2 / (4\kappa m)$ of these regions, we have only one solution as given by

$$M_1 = M_2 = \frac{\hat{\Sigma}}{4\kappa m} = \frac{\Sigma + 2\kappa m^2}{4\kappa m}. \tag{5.75}$$

For all other possible values of $\hat{\Sigma}$ and ΔP, we have two different solutions as in Eq. 5.72 with $M_1 \neq M_2$, corresponding to two different spherical segments. In general, the mean curvatures M_1 and M_2 may be positive or negative depending on the signs of the pressure difference ΔP, the membrane tension Σ, and the spontaneous curvature m.

Coexistence of two spherical segments

The two solutions M_1 and M_2 are characterized by the same values of the pressure difference ΔP and the mechanical tension Σ. Therefore, the two membrane segments can coexist for these values of ΔP and Σ. Vice versa, when we observe the coexistence of two spherical membrane segments with mean curvatures M_1 and M_2, we can use the two Euler-Lagrange equations to conclude that the membrane tension is given by

$$\Sigma = 2\kappa m(M_1 + M_2) - 2\kappa m^2 \tag{5.76}$$

and the pressure difference by

$$\Delta P = 4\kappa m M_1 M_2. \tag{5.77}$$

The coexistence of two spherical shapes is indeed observed when out- and in-buds are formed from larger mother vesicles as shown in Figure 5.2 through Figure 5.6 and discussed in more detail in the next subsection.

On the other hand, the coexistence of more than two spherical segments with pair-wise different mean curvatures M_i and M_j is not possible for a uniform membrane. Indeed, if $N \geq 3$ different types of spherical segments coexisted on the same vesicle, we would have N Euler-Lagrange equations of the form Eq. 5.70. When we now choose a pair of spherical segments with mean curvatures M_i and M_j, we obtain the relations Eqs 5.76 and 5.77 with M_1 and M_2 replaced by M_i and M_j. For fixed i, we can choose $N - 1$ different values for j and obtain $N - 1$ different relations of the form Eqs 5.76 and 5.77. These relations immediately imply that all mean curvatures M_j must be identical. Because we can repeat this procedure for each value of i, we conclude that the shape equations for spherical segments allow only two different values of the mean curvature to coexist for uniform membranes.

Multi-component membranes can lead to the coexistence of several lipid phases and several types of intramembrane domains that differ in their composition, see Section 5.8 below. For two types of domains, the membrane can form coexisting spherical segments with four different mean curvatures. In general, a membrane with K types of domains can form coexisting spherical segments with $2K$ different mean curvatures as follows from the Euler-Lagrange equations for the different membrane domains. This morphological complexity remains to be explored.

Stability of individual spheres

Now, consider a single sphere which experiences the pressure difference $P_{sp} = P_{sp,in} - P_{sp,ex}$ where $P_{sp,in}$ is the osmotic pressure acting within the volume enclosed by the sphere. The second variation of the shape functional shows that a sphere with radius R_{sp} and mean curvature $M = 1/R_{sp}$ is (locally) stable provided this pressure difference P_{sp} satisfies (Ou-Yang and Helfrich, 1989; Seifert et al., 1991; Miao et al., 1991)

$$P_{sp} > P_{sp}^{*+} \equiv \frac{4\kappa}{R_{sp}^3}(mR_{sp} - 3) \quad (M_{sp} = 1/R_{sp}) \tag{5.78}$$

When we reverse the normal vector of the sphere, we change the signs of both the mean curvature M and the spontaneous curvature m. For such an inverted sphere, we obtain the stability condition

$$P_{sp} > P_{sp}^{*-} \equiv \frac{4\kappa}{R_{sp}^3}(-mR_{sp} - 3) \quad (M_{sp} = -1/R_{sp}). \tag{5.79}$$

One example for an inverted sphere in real systems is provided by an in-bud protruding into a giant vesicle which is a possible shape for negative spontaneous curvature $m < 0$. The in-bud with radius $R_{sp} = R_2$ and mean curvature $M_2 = -1/R_2$ is attached to a spherical mother vesicle with radius $R_{sp} = R_1 \geq R_2$ and mean curvature $M_1 = 1/R_1$. In this case, the volume enclosed by the in-bud is a subvolume of the exterior solution. Therefore, the membrane of the in-bud experiences the pressure difference $P_{sp} = -\Delta P$ whereas the membrane of the mother vesicle is exposed to $P_{sp} = \Delta P$.

Because the mother vesicle and the in-bud experience two different pressure differences, the two spherical membrane segments are then governed by two different stability conditions. Indeed, using the stability relations Eqs 5.78 and 5.79 as well as the general expression Eq. 5.77 for ΔP, the spherical shape of the mother vesicle is found to be stable if

$$\Delta P = -\frac{4\kappa m}{R_1 R_2} > \frac{4\kappa}{R_1^3}(mR_1 - 3) \quad \text{or} \quad \frac{m}{R_2} < \frac{3 - mR_1}{R_1^2} \tag{5.80}$$

whereas the stability condition for the spherical in-bud has the form

$$-\Delta P = \frac{4\kappa m}{R_1 R_2} > \frac{4\kappa}{R_2^3}(-mR_2 - 3) \text{ or } \frac{m}{R_1} > \frac{-mR_2 - 3}{R_2^2} \tag{5.81}$$

At the critical pressures $P_{sp} = P_{sp}^{*\pm}$, the spherical shape undergoes a bifurcation which generates the branches of prolate and oblate shapes. For conventional spheres with $M_{sp} > 0$, the prolate shape has the lowest bending energy for small $|m|/M_{sp}$-values whereas the oblate shape represents the lower energy shape for sufficiently large negative values of m/M_{sp}, see the morphology diagram in Figure 5.16 (Seifert et al., 1991).

5.5.2 TWO-SPHERE VESICLES

Giant vesicles frequently form shapes that consist of two spheres connected by a narrow membrane neck. Within the spontaneous curvature model, such shapes arise quite naturally and can be reached by deflation of smoothly curved shapes. Two such limit shapes have been obtained from a systematic numerical study of axisymmetric shapes (Berndl, 1990; Seifert et al., 1991): the limit shapes L^{pea} with a spherical out-bud and the limit shapes L^{sto} with a spherical in-bud. These limit shapes represent two-sphere shapes and have the geometries displayed in Figure 5.15. The limit shapes L^{pea} are reached, for positive spontaneous curvature, by the deflation of pear-like vesicles, the limit shapes L^{sto} for negative spontaneous curvature by the deflation of stomatocytes, see the morphology diagram in Figure 5.16. Inspection of this diagram shows that these limit shapes are found along two lines within the $(v, \bar{m})$-plane.

Closer inspection of this morphology diagram also reveals that the deflation of a spherical vesicle with $v = 1$ and $\bar{m} > 0$ leads to a prolate-pear bifurcation before the limit shape L^{pea} is reached. Because the latter bifurcation is discontinuous and exhibits hysteresis, the experimental observation of the true limit shape will be facilitated if one studies both the deflation and the subsequent inflation of the GUV. Likewise, the deflation of a spherical vesicle with $v = 1$ and $\bar{m} < 0$ leads to an oblate-stomatocyte bifurcation

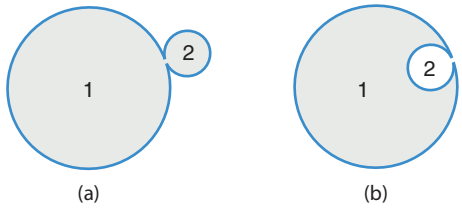

Figure 5.15 Geometry of shapes consisting of two spheres with radii $r_1 = R_1/R_{ve}$ and $r_2 = R_2/R_{ve} \leq r_1$ connected by a closed neck: (a) Two-sphere shape Θ^{out} with an out-bud and *positive* neck curvature $\bar{M}_{ne} = \frac{1}{2}(\frac{1}{r_1} + \frac{1}{r_2}) > 0$ which can only form for positive spontaneous curvature $\bar{m} \geq \sqrt{2}$ and (b) Two-sphere shape Θ^{in} with an in-bud and *non-positive* neck curvature $\bar{M}_{ne} = \frac{1}{2}(\frac{1}{r_1} - \frac{1}{r_2}) \leq 0$ which can only form for non-positive spontaneous curvature $\bar{m} \leq 0$. The stability of the membrane neck in (a) and (b) is governed by Eqs 5.60 and 5.61, respectively. $\bar{M}_{ne} = \bar{m}$, the shape Θ^{out} in (a) represents a limit shape L^{pea} as obtained by neck closure from a stationary pear-like shape of the Euler-Lagrange equation while it represents a persistent shape Φ^{pea} with a stably closed neck for $\bar{M}_{ne} < \bar{m}$. Likewise, the shape Θ^{in} may represent a limit shape L^{sto} as obtained by neck closure from a stationary stomatocyte or a persistent shape Φ^{sto}. The limit shapes are found along certain lines within the $(v, \bar{m})$-plane whereas the persistent shapes are stable within two-dimensional regions of this plane, see the morphology diagrams in Figures 5.16 and 5.17.

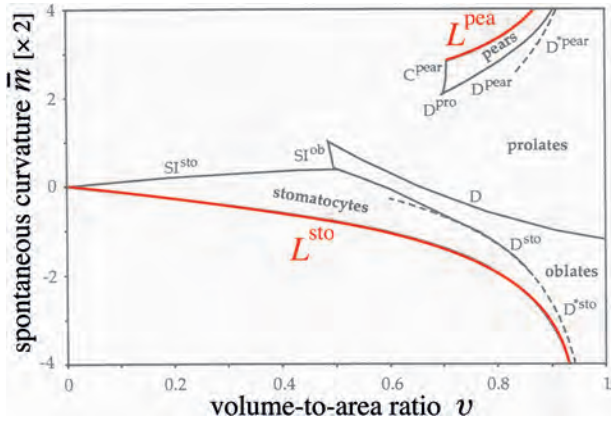

Figure 5.16 Morphology diagram as a function of volume-to-area ratio v and spontaneous curvature $c_0 \equiv 2\bar{m}$ which exhibits two lines of limit shapes. The limit shapes L^{pea} with an out-bud as in Figure 5.15a are found for $\bar{m} \geq \sqrt{2}s$ along the upper line which is truncated at the end point $(v_*^+, \bar{m}_*^+) = (1/\sqrt{2}, \sqrt{2})$ corresponding to two equal spheres. As we move along the L^{pea}-line by increasing the spontaneous curvature $\bar{m}$ and the volume-to-area-ratio v, the out-bud becomes smaller and smaller until the whole membrane area is taken up by the larger sphere. The limit shapes L^{sto} with an out-bud, see Figure 5.15b, are found for $\bar{m} \leq 0$ along the lower line which is truncated at the end point $(v_*^-, \bar{m}_*^-) = (0,0)$ corresponding to two nested spheres of equal size. As we move along the L^{sto}-line by decreasing $\bar{m} < 0$ and increasing v, the in-bud becomes smaller and smaller until the vesicle forms a single sphere with $v = 1$ (Berndl, 1990). (Reproduced from Seifert, U. et al., *Phys. Rev. A*, 44, 1182–1202, 1991; Berndl, K. *Formen Von Vesikeln Diplomarbeit*, Ludwig–Maximilians–Universität München, 1990.)

before the limit shape L^{sto} is reached. The latter bifurcation is again discontinuous (Seifert et al., 1991).

The following analysis of two-sphere vesicles involves several steps (Lipowsky, 2018b). First, the geometric properties of the two-sphere shapes lead to other types of limit shapes, $L_{=}^{out}$ and

$L_{=}^{\text{in}}$, consisting of two identical spheres. Second, the neck closure condition determines the limit shapes L^{pea} and L^{sto}. Finally, we must examine the stability of the two individual spheres in order to find instability lines at which the two-sphere vesicles transform into other types of shapes. We will also emphasize two-sphere vesicles with buds that have zero bending energy and consider the two-sphere limit shapes obtained in the presence of area difference elasticity.

Geometric properties

The geometry of any two-sphere vesicle is determined by the radii R_1 and R_2 of the two spheres. In the following, we will consider vesicles with fixed area A and vesicle size $R_{\text{ve}} = \sqrt{A/(4\pi)}$ but variable volume V as controlled by the osmotic conditions. We then measure the radii of the two spheres in units of R_{ve} and define the dimensionless radii

$$r_1 \equiv R_1 / R_{\text{ve}} \quad \text{and} \quad r_2 \equiv R_2 / R_{\text{ve}}. \tag{5.82}$$

These two radii satisfy the implicit equations

$$r_1^2 + r_2^2 = \frac{A}{4\pi R_{\text{ve}}^2} = 1 \tag{5.83}$$

and

$$r_1^3 \pm r_2^3 = \frac{V}{\frac{4\pi}{3} R_{\text{ve}}^3} = v \tag{5.84}$$

where the plus and minus sign in Eq. 5.84 correspond to two-sphere shapes with an out- and in-bud, respectively. Therefore, the geometry of any two-sphere vesicle is determined by its area A and its volume V and depends only on the volume-to-area ratio v. As in Figure 5.15, we use the notation Θ^{out} and Θ^{in} for two-sphere shapes for which we have not examined the stability of their necks.

For a two-sphere vesicle with an in-bud, the radius r_2 of this bud must satisfy $r_2 \le r_1$ because the membrane segments of the two spheres should not intersect. For a two-sphere vesicle with an out-bud, the shapes for $r_1 < r_2$ are identical with the shapes for $r_1 > r_2$. In order to avoid this degeneracy, we will impose the restriction $r_2 \le r_1$ for out-buds as well. Because $r_1^2 + r_2^2 = 1$ as in Eq 5.83, the inequality $r_1 \ge r_2 = \sqrt{1 - r_1^2}$ implies

$$r_1 \ge \frac{1}{\sqrt{2}} \quad \text{and} \quad r_2 \le \frac{1}{\sqrt{2}}. \tag{5.85}$$

The limiting cases with $r_2 = r_1 = 1/\sqrt{2}$ corresponds to two spheres with the same size and defines two other types of limit shapes, denoted by $L_{=}^{\text{out}}$ and $L_{=}^{\text{in}}$. The limit shape $L_{=}^{\text{out}}$ consists of two equal spheres with positive mean curvature whereas the limit shape $L_{=}^{\text{in}}$ consists of two nested spheres which have the same size but opposite mean curvatures. In addition, these limit shapes have the smallest possible volume of two-sphere vesicles as given by

$$\min(v) = v_{=}^{\text{out}} \equiv 1/\sqrt{2} \quad \text{for } L_{=}^{\text{out}} \tag{5.86}$$

and

$$\min(v) = v_{=}^{\text{in}} \equiv 0 \quad \text{for } L_{=}^{\text{in}}. \tag{5.87}$$

A related property of these limit shapes is that their neck curvatures have the smallest absolute values. When expressed in terms of the dimensionless neck curvature

$$\bar{M}_{\text{ne}} \equiv M_{\text{ne}} R_{\text{ve}} = \frac{1}{2}\left(\frac{1}{r_1} \pm \frac{1}{r_2}\right), \tag{5.88}$$

these minimal neck curvatures have the values

$$\min(\bar{M}_{\text{ne}}) = \sqrt{2} \quad \text{for } L_{=}^{\text{out}} \tag{5.89}$$

and

$$\min(|\bar{M}_{\text{ne}}|) = \max(\bar{M}_{\text{ne}}) = 0 \quad \text{for } L_{=}^{\text{in}}. \tag{5.90}$$

Neck closure and neck stability

A necessary prerequisite for a stable two-sphere vesicle is the stability of the closed neck connecting the two spheres. The stability of closed necks was already studied in subsection 5.4.6 where we distinguished neck closure from closed neck conditions. The closure condition has the dimensionless form

$$\bar{M}_{\text{ne}} = \frac{1}{2}\left(\frac{1}{r_1} \pm \frac{1}{r_2}\right) = \bar{m} \quad \text{(neck closure)} \tag{5.91}$$

where the plus and minus sign again corresponds to two-sphere shapes with out- and in-buds, respectively. In addition, the closed neck condition is given by

$$0 < \bar{M}_{\text{ne}} = \frac{1}{2}\left(\frac{1}{r_1} + \frac{1}{r_2}\right) < \bar{m} \quad \text{for out-buds} \tag{5.92}$$

and by

$$0 > \bar{M}_{\text{ne}} = \frac{1}{2}\left(\frac{1}{r_1} - \frac{1}{r_2}\right) > \bar{m} \quad \text{for in-buds.} \tag{5.93}$$

Limit shapes related to neck closure

The combination of the geometric relations Eqs 5.83 and 5.84 with the neck closure condition Eq. 5.91 determines the limit shapes L^{pea} and L^{sto}. When we eliminate the two radii from these three equations, we obtain the functional relationships

$$v = v^{\text{pea}}(\bar{m}) \quad \text{for the line of } L^{\text{pea}} \text{ shapes} \tag{5.94}$$

and

$$v = v^{\text{sto}}(\bar{m}) \quad \text{for the line of } L^{\text{sto}} \text{ shapes.} \tag{5.95}$$

The function $v^{\text{pea}}(\bar{m})$ has the explicit form (Seifert et al., 1991)

$$v = v^{\text{pea}}(\bar{m}) \equiv -\frac{1}{4\bar{m}^3} + \left(1 - \frac{1}{2\bar{m}^2}\right)\sqrt{1 + \frac{1}{4\bar{m}^2}} \quad \text{for} \quad \bar{m} \geq \sqrt{2}, \quad (5.96)$$

which behaves as

$$v^{\text{pea}}(\bar{m}) \approx 1 - \frac{3}{8\bar{m}^2} \quad \text{for large } \bar{m}. \quad (5.97)$$

The function $v^{\text{sto}}(\bar{m})$ has the same $\bar{m}$-dependence as $v^{\text{pea}}(\bar{m})$ but applies to $\bar{m} \leq 0$.

Both lines of limit shapes L^{pea} and L^{sto} extend down to the smallest possible volumes which they reach when both spheres have the same size. The corresponding values of the spontaneous curvature $\bar{m}$ are given by

$$\min(\bar{m}) = \bar{m}_{=}^{\text{out}} \equiv \sqrt{2} \quad \text{for } L^{\text{pea}} \quad (5.98)$$

and by

$$\max(\bar{m}) = \bar{m}_{=}^{\text{in}} \equiv 0 \quad \text{for } L^{\text{sto}}, \quad (5.99)$$

see the L^{pea} and L^{sto} lines in Figure 5.16. In the following subsection, the region of the morphology diagram with $\bar{m} > 0$, which contains the limit shapes L^{pea} and $L_{=}^{\text{out}}$, will be discussed in more detail.

Buds with zero bending energy

It is useful to distinguish another special case of budded vesicle shapes, denoted by Z^{out} and Z^{in}. The spherical buds of these shapes have radius $r_2 = 1/|\bar{m}|$ and thus zero bending energy. Because of the inequality $r_2 \leq 1/\sqrt{2}$ as in Eq. 5.85, we then have

$$r_2 = \frac{1}{|\bar{m}|} \leq \frac{1}{\sqrt{2}} \quad \text{and} \quad r_1 = \sqrt{1 - \frac{1}{\bar{m}^2}} \geq \frac{1}{\sqrt{2}}. \quad (5.100)$$

Both relations lead to the same inequality $|\bar{m}| \geq \sqrt{2}$ which implies

$$\bar{m} \geq \sqrt{2} \quad \text{for out-buds} \quad (5.101)$$

and

$$\bar{m} \leq -\sqrt{2} \quad \text{for in-buds.} \quad (5.102)$$

For these vesicles, the buds have vanishing bending energy and the whole bending energy is provided by the bending energy of the mother vesicle with radius r_1. The neck mean curvature is then given by

$$\bar{M}_{\text{ne}} = \bar{M}_{\text{ne}}^0(\bar{m}) \equiv \frac{1}{2}\left(\frac{1}{\sqrt{1 - 1/\bar{m}^2}} + \bar{m}\right) \quad (5.103)$$

which satisfies

$$\bar{M}_{\text{ne}}^0(\bar{m}) \leq \bar{m} \quad \text{for out-buds with } \bar{m} \geq \sqrt{2} \quad (5.104)$$

and

$$\bar{M}_{\text{ne}}^0(\bar{m}) \geq \bar{m} \quad \text{for in-buds with } \bar{m} \leq -\sqrt{2}. \quad (5.105)$$

Comparison with the stability relations as given by Eqs 5.92 and 5.93 then shows that the closed necks between the zero-energy buds and the mother vesicles are stable for both positive and negative spontaneous curvatures. For out-buds, the equality $\bar{M}_{\text{ne}} = \bar{M}_{\text{ne}}^0(\bar{m}) = \bar{m}$ describes the neck closure condition and applies to $r_1 = r_2 = 1/\bar{m}$, i.e., to the case of two identical spheres. This special morphology represents a limit shape for which the whole bending energy vanishes.

The volume of the two-sphere vesicles Z^{out} and Z^{in} with zero-energy buds is given by

$$v = v^{\text{zeb}} \equiv \left(1 - \frac{1}{\bar{m}^2}\right)^{3/2} \pm \frac{1}{\bar{m}^3} \quad (5.106)$$

where the plus and minus sign applies to out- and in-buds, respectively. This volume behaves as

$$v^{\text{zeb}} \approx 1 - \frac{3}{2\bar{m}^2} \quad \text{for large } |\bar{m}| \quad (5.107)$$

which applies to both out-buds with $\bar{m} > 0$ and in-buds with $\bar{m} < 0$.

Morphology diagram for positive spontaneous curvature

As displayed in Figure 5.17, the morphology diagram for positive spontaneous curvature contains two lines of limit shapes, L^{pea} and $L_{=}^{\text{out}}$, that have a common end point at

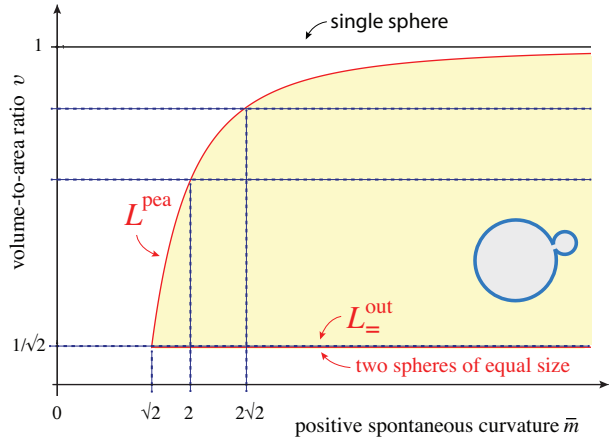

Figure 5.17 Morphology diagram for two-sphere vesicles with an out-bud (inset) and positive spontaneous curvature: Such vesicles have *positive* neck curvature and can be formed for spontaneous curvature $\bar{m} \geq \sqrt{2}$ as well as reduced volume v in the interval $1/\sqrt{2} \leq v \leq v^{\text{pea}}(\bar{m})$ corresponding to the shaded (yellow) region. The lower boundary of this region (horizontal line) is provided by the limit shapes $L_{=}^{\text{out}}$ that consist of two identical spheres and have the volume $v_{=}^{\text{out}} = 1/\sqrt{2}$, the upper boundary (curved line) by the limit shapes L^{pea} as described by $v = v^{\text{pea}}(\bar{m})$ in Eq. 5.96. The two boundary lines have a common end point at $(\bar{m}_{=}^{\text{out}}, v_{=}^{\text{out}}) = (\sqrt{2}, 1/\sqrt{2})$. When a limit shape L^{pea} is deflated for constant spontaneous curvature $\bar{m} > \sqrt{2}$, the larger sphere shrinks whereas the smaller sphere (or out-bud) grows transforming the limit shape L^{pea} into a persistent shape Φ^{pea} with neck curvature $\bar{M}_{\text{ne}} < \bar{m}$. The closed neck persists during further deflation until the lower limit shape $L_{=}^{\text{out}}$ with two identical spheres is reached. All two-sphere vesicles with the same volume v (broken horizontal lines) have the same neck curvature and the same shape but differ in their bending energy, see text. The upper broken line corresponds to the two-sphere geometry with $v = 0.941$ and $\bar{M}_{\text{ne}} = 2\sqrt{2}$, the intermediate broken line to $v = 0.871$ and $\bar{M}_{\text{ne}} = 2$.

$(\bar{m},v)=(\bar{m}_{=}^{\text{out}},v_{=}^{\text{out}})=(\sqrt{2},1/\sqrt{2})$. Thus, the limit shapes L^{pea} are located at

$$v=v^{\text{pea}}(\bar{m}) \quad \text{and} \quad \bar{m}\geq\bar{m}_{=}^{\text{out}}=\sqrt{2} \tag{5.108}$$

while the $L_{=}^{\text{out}}$ shapes are located at

$$v=v_{=}^{\text{out}}=1/\sqrt{2} \quad \text{and} \quad \bar{m}\geq\bar{m}_{=}^{\text{out}}=\sqrt{2}. \tag{5.109}$$

Note that all $L_{=}^{\text{out}}$ shapes have the same geometry but differ in their bending energy which has the $\bar{m}$-dependent form

$$\bar{E}_{\text{be}}\{L_{=}^{\text{out}}\}=\frac{E_{\text{be}}\{L_{=}^{\text{out}}\}}{8\pi\kappa}=2(1-\eta_1\bar{m})^2 \quad \text{with } \eta_1=1/\sqrt{2}. \tag{5.110}$$

which vanishes for $\bar{m}=\bar{m}_{=}^{\text{out}}=\sqrt{2}$ and increases as $\sim\bar{m}^2$ for large $\bar{m}$.

Inspection of Figure 5.17 shows that the two lines of limit shapes enclose an extended region of two-sphere shapes, Φ^{pea}, with stably closed necks. This region can be entered by deflation of the L^{pea} shapes, by inflation of the $L_{=}^{\text{out}}$ shapes, and by increasing the spontaneous curvature of the L^{pea} shapes. All Φ^{pea} shapes that are produced by one of these processes are persistent in the sense that their necks remain stably closed during both deflation and inflation as well as under small changes of the spontaneous curvature.

Stability of individual spheres

A second requirement for the stability of two-sphere vesicles is the shape stability of both spheres. Thus, in order to examine the stability of the individual spheres, we now use the stability criterion Eq. 5.78 together with the pressure difference $P_{\text{sp}}=\Delta P$ and ΔP as given by Eq. 5.77. We then conclude that the spherical mother vesicle with radius R_1 is stable if

$$\Delta P=\frac{4\kappa m}{R_1R_2}>\frac{4\kappa}{R_1^3}(mR_1-3) \quad \text{or} \quad \frac{\bar{m}}{r_2}>\frac{\bar{m}\eta_1-3}{\eta_1^2} \tag{5.111}$$

whereas the out-bud with radius R_2 is stable if

$$\Delta P=\frac{4\kappa m}{R_1R_2}>\frac{4\kappa}{R_2^3}(mR_2-3) \quad \text{or} \quad \frac{\bar{m}}{\eta_1}>\frac{\bar{m}r_2-3}{r_2^2}. \tag{5.112}$$

Because the two radii $r_1=R_1/R_{\text{ve}}$ and $r_2=R_2/R_{\text{ve}}$ satisfy the geometric relation $r_1^2+r_2^2=1$, we can express both stability relations in terms of a single radius, say r_2. One then finds that both individual spheres are stable for all limit shapes L^{pea} and $L_{=}^{\text{out}}$ as well as for the shapes Z^{out} with zero-energy buds. Furthermore, the larger sphere of the intermediate persistent shapes Φ^{pea} is always stable whereas the spherical out-bud may become unstable for sufficiently large values of the spontaneous curvature and a certain range of v-values. More precisely, the spherical out-bud with radius r_2 is stable if

$$r_2-\frac{r_2^2}{\sqrt{1-r_2^2}}<\frac{3}{\bar{m}} \tag{5.113}$$

and unstable if

$$r_2-\frac{r_2^2}{\sqrt{1-r_2^2}}>\frac{3}{\bar{m}}. \tag{5.114}$$

Therefore, the instability line between the stable and unstable out-buds follows from the solutions of the equation

$$r_2-\frac{r_2^2}{\sqrt{1-r_2^2}}=\frac{3}{\bar{m}}. \tag{5.115}$$

This equation has no solution for $\bar{m}<\bar{m}_{\text{ss}}=13.29$, one solution for $\bar{m}=\bar{m}_{\text{ss}}$ and two solutions for $\bar{m}>\bar{m}_{\text{ss}}$.

Therefore, the out-buds of the persistent shapes Φ^{pea} are stable for $\bar{m}<\bar{m}_{\text{ss}}$ but become unstable for $\bar{m}\geq\bar{m}_{\text{ss}}$ and a certain $\bar{m}$-dependent range of v-values. At $\bar{m}=\bar{m}_{\text{ss}}$, the instability consists of the single point $(\bar{m}_{\text{ss}},v_{\text{ss}})=(13.29,0.8259)$ which opens up into a parabola-like curve for $\bar{m}>\bar{m}_{\text{ss}}$. For large $\bar{m}$, the upper and lower branches of the parabola-like curve approach the Z^{out} line and the $L_{=}^{\text{out}}$ line, respectively. Because $\bar{m}_{\text{ss}}=13.29$, this bifurcation structure is located outside of the $(\bar{m},v)$-region displayed in Figure 5.17.

Thus, we conclude that two-sphere vesicles with out-buds can be found in a large region of the morphology diagram for $\bar{m}>0$. In particular, when we deflate a limit shape L^{pea} for $\sqrt{2}<\bar{m}<\bar{m}_{\text{ss}}\simeq 13.29$, we obtain a family of stable persistent shapes Φ^{pea} with decreasing neck curvatures $\bar{M}_{\text{ne}}$ until we reach the limit shape $L_{=}^{\text{out}}$ with the smallest possible neck curvature $\bar{M}_{\text{ne}}=\bar{m}_{*}^{+}=\sqrt{2}$. Further deflation of the limit shape $L_{=}^{\text{out}}$ leads back to a dumbbell-like shape with an open neck.

5.5.3 MODIFICATIONS BY AREA DIFFERENCE ELASTICITY

So far, two-sphere vesicles have been discussed in the context of the spontaneous curvature model which depends on the locally generated spontaneous curvature m and assumes that one molecular component of the bilayer membrane can undergo frequent flip-flops between the two bilayer leaflets. It is instructive to see how the morphology diagram is changed when we consider bilayer membranes with slow flip-flops between the leaflets. In the latter situation, the area difference ΔA between the two leaflets is constrained as described by the nonlocal energy term in the area-difference-elasticity model, see the nonlocal expression in Eq. 5.64 that contributes to the energy functional Eq. 5.63 of this model.

As explained in Section 4.7.1, the shapes that minimize this energy functional also minimize the energy functional of the spontaneous curvature model as in Eq. 5.12, provided we use the effective spontaneous curvature $m_{\text{eff}}\equiv m+m_{\text{nlo}}$ as given by Eq. 5.66 which represents the sum of the local spontaneous curvature m and the nonlocal spontaneous curvature

$$m_{\text{nlo}}\equiv\pi\frac{\kappa_\Delta}{\kappa}\frac{I_{M,0}-\mathcal{I}_M\{S\}}{A}$$

as in Eq. 5.67. If the leaflets of a sphere with radius R_{ve} have optimal molecular areas, one has $I_{M,0} = 4\pi R_{ve}$ and the geometric factor of the nonlocal spontaneous curvature becomes

$$\frac{I_{M,0} - \mathcal{I}_M\{S\}}{\mathcal{A}} = \frac{4\pi R_{ve} - \mathcal{I}_M\{S\}}{4\pi R_{ve}^2}. \tag{5.116}$$

Now, consider again the two-sphere vesicles Θ^{out} and Θ^{in} with radii R_1 and R_2 connected by a closed membrane neck as shown in Figure 5.15. The integrated mean curvature $\mathcal{I}_M$ of these shapes is given by

$$\mathcal{I}_M\{\Theta^{out}\} = 4\pi(R_1 + R_2) \quad \text{and} \quad \mathcal{I}_M\{\Theta^{in}\} = 4\pi(R_1 - R_2) \tag{5.117}$$

which leads to the geometric factors

$$\frac{4\pi R_{ve} - \mathcal{I}_M\{S\}}{4\pi R_{ve}^2} = \frac{1}{R_{ve}}(1 - r_1 \mp r_2) \tag{5.118}$$

and to the nonlocal spontaneous curvatures

$$\bar{m}_{nlo} = m_{nlo} R_{ve} = \pi \frac{\kappa_\Delta}{\kappa}(1 - r_1 \mp r_2) \tag{5.119}$$

where the minus and plus sign applies to out- and in-buds, respectively. The nonlocal spontaneous curvature involves the geometric factor

$$1 - r_1 \mp r_2 = 1 - r_1 \mp \sqrt{1 - r_1^2} \tag{5.120}$$

where we used the area relation $r_1^2 + r_2^2 = 1$. For the shape Θ^{out} with an out-bud, this expression is negative and bounded by

$$1 - \sqrt{2} \le 1 - r_1 - \sqrt{1 - r_1^2} \le 0 \quad \text{for } 0 \le r_1 \le 1 \text{ (out-bud)}. \tag{5.121}$$

For the shape Θ^{in} with an in-bud, on the other hand, the corresponding expression is positive and satisfies the bounds

$$0 \le 1 - r_1 + \sqrt{1 - r_1^2} \le \sqrt{2} + 1 \quad \text{for } 0 \le r_1 \le 1 \text{ (in-bud)}. \tag{5.122}$$

Therefore, the absolute value of the nonlocal spontaneous curvature satisfies the bounds

$$|\,\bar{m}_{nlo}\,| \le \pi(\sqrt{2} - 1)\frac{\kappa_\Delta}{\kappa} \quad \text{for } \Theta^{out} \tag{5.123}$$

and

$$|\,\bar{m}_{nlo}\,| \le \pi(\sqrt{2} + 1)\frac{\kappa_\Delta}{\kappa} \quad \text{for } \Theta^{in}. \tag{5.124}$$

These bounds can be used to estimate the relative magnitude of the nonlocal and local contributions to the spontaneous curvature, see further below.

When we include area-difference-elasticity, the stability conditions for the closed neck are given by Eqs 5.68 and 5.69 which imply the neck closure condition

$$\bar{M}_{ne} = \frac{1}{2}\left(\frac{1}{r_1} \pm \frac{1}{r_2}\right) = \bar{m} + \bar{m}_{nlo} = \bar{m} + \pi \frac{\kappa_\Delta}{\kappa}(1 - r_1 \mp r_2) \tag{5.125}$$

where the last equality follows from Eq. 5.119. In order to determine the location of the limit shapes L^{pea} and L^{sto} in the $(v, \bar{m})$-plane, we must now combine the neck closure relation Eq 5.125 with the geometric relations $r_1^2 + r_2^2 = 1$ and $r_1^3 \pm r_2^3 = v$. In general, the κ_Δ-term will shift the L^{pea}- and L^{sto}-lines in the $(v, \bar{m})$-plane, a shift that can be easily calculated for any value of κ_Δ/κ. For positive spontaneous curvature, for example, one then finds that the lines of limit shapes L^{pea} are shifted towards higher $\bar{m}$-values as we increase the rigidity ratio κ_Δ/κ. Furthermore, when we describe the shifted L^{pea} lines by $\bar{m}^{pea} = f(v)$. the function $f(v)$ develops a minimum for $\kappa_\Delta/\kappa > 1$.

In addition, we can draw some general conclusions about the morphology diagram when we include the area-difference-elasticity term proportional to κ_Δ. First, the limit shapes $L_=^{out}$ and $L_=^{in}$, consisting of two spheres with the same radius, are again located at $v = v_=^{out} = 1/\sqrt{2}$ for $\bar{m} > 0$ and at $v = v_=^{in} = 0$ for $\bar{m} < 0$ as follows from the two geometric relations alone. Therefore, the morphology diagram in the $(v, \bar{m})$-plane will always contain extended regions with (meta)stable two-sphere shapes as in Figure 5.17, irrespective of the value of κ_Δ/κ.

Second, we can conclude from the neck closure condition in Eq. 5.125 and from the bounds provided by Eqs 5.123 and 5.124 that the nonlocal contributions $\bar{m}_{nlo}$ arising from area difference elasticity can be neglected for sufficiently large local contributions $\bar{m}$. More precisely, we obtain from Eqs 5.125 and 5.123 that the nonlocal spontaneous curvature can be ignored for the shape Θ^{out} if the local spontaneous curvature is sufficiently large and positive with

$$\bar{m} \gg \pi(\sqrt{2} - 1)\frac{\kappa_\Delta}{\kappa} \quad \text{(out-bud)}. \tag{5.126}$$

Likewise, combining Eq. 5.125 with Eq. 5.124, we conclude that the nonlocal contribution can be ignored for the shape Θ^{in} if the local spontaneous curvature is large and negative with

$$\bar{m} \ll -\pi(\sqrt{2} + 1)\frac{\kappa_\Delta}{\kappa} \quad \text{(in-bud)}. \tag{5.127}$$

The ratio κ_Δ/κ of the bending rigidities is expected to be of the order of one (Döbereiner et al., 1997). Therefore, both for out- and for in-buds, the nonlocal contribution can be ignored compared to the local one if $|\,\bar{m}\,| \gg 1$ or $|\,m\,| \gg 1/R_{ve}$.

Finally, assume that we were able to measure the radii r_1 and r_2 of a vesicle during neck closure. We can then use the neck closure condition in Eq. 5.125 to estimate the local spontaneous curvature $\bar{m}$ via

$$\bar{m} = \frac{1}{2}\left(\frac{1}{r_1} \pm \frac{1}{r_2}\right) + \pi \frac{\kappa_\Delta}{\kappa}(r_1 \pm r_2 - 1) \tag{5.128}$$

where the plus and minus sign applies to an out- and in-bud, respectively. For small bud radius r_2, the radius $r_1 = \sqrt{1-r_2^2} \approx 1 - r_2^2$. When we use this asymptotic equality in Eq. 5.128, we obtain the local spontaneous curvature which implies

$$\bar{m} \approx \frac{1}{2}\left(\frac{1}{r_1} \pm \frac{1}{r_2}\right) \pm \pi \frac{\kappa_\Delta}{\kappa} r_2 \quad \text{for small buds with } r_2 \ll 1. \tag{5.129}$$

The asymptotic behavior as given by Eq. 5.129 implies that the κ_Δ-term can also be ignored for sufficiently small buds. This behavior for small buds is consistent with the behavior for large spontaneous curvatures $\bar{m}$ because large $\bar{m}$ implies limit shapes with small buds.

The influence of area difference elasticity on two-sphere vesicles has been recently studied for giant vesicles that contained lipids with photoresponsive F-Azo groups and underwent light-induced budding (Georgiev et al., 2018). A theoretical analysis of the experimental data based on Eq. 5.128 showed that the spontaneous curvature can indeed be decomposed into a local and a nonlocal contribution, that all vesicles were governed by the same rigidity ratio κ_Δ/κ, and that the local spontaneous curvature $m = \bar{m}R_{ve}$ was about 1/(2.5 μm).

5.5.4 EFFECTIVE CONSTRICTION FORCES AND CLEAVAGE OF MEMBRANE NECKS

As explained in the previous subsections, the persistent shapes Φ^{pea} have the same geometry, for a given volume v, as the limit shapes L^{pea} but an increased spontaneous curvature $\bar{m}$ compared to the spontaneous curvature of L^{pea}. When expressed in terms of dimensionful variables, the spontaneous curvature m then satisfies the stability condition $m > M_{ne} = \frac{1}{2}(M_1 + M_2)$ for the closed necks of out-buds as in Eqs 5.60 and 5.92. Now, consider an explicit constriction force f that acts on the neck radius R_{ne}, which we take into account by adding the term fR_{ne} to the bending energy in Eq. 5.54.[10] We then obtain the generalized condition

$$f - 4\pi\kappa(M_1 + M_2 - 2m) > 0 \tag{5.130}$$

for a closed membrane neck which may be rewritten in the form

$$f + f_{eff}^{out} > 0 \tag{5.131}$$

with the effective constriction force

$$f_{eff}^{out} \equiv 4\pi\kappa(2m - M_1 - M_2) \geq 0 \quad \text{(out-buds with } m > 0). \tag{5.132}$$

This constriction force vanishes when the neck satisfies the neck closure condition $M_1 + M_2 = 2m$.

Now, let us consider a persistent shape Φ^{pea} close to the line of limit shapes $L_=^{out}$ which consist of two identical spheres. These persistent shapes have a volume $v \gtrsim 1/\sqrt{2}$ and are characterized by two spheres with small mean curvatures M_1 and M_2, both of which are of the order of $\sqrt{2}/R_{ve}$. Furthermore, the individual spheres of these persistent shapes are stable up to fairly high m-values because the individual spheres of the limit shapes $L_=^{out}$ are stable for all values of m. If the spontaneous curvature m is large compared to both M_1 and M_2, the expression for the curvature-induced constriction force as given by Eq. 5.132 simplifies and becomes asymptotically equal to

$$f_{eff}^{out} \approx f_m^{out} \quad \text{with} \quad f_m^{out} \equiv 8\pi\kappa m \quad \text{for } 2m \gg M_1 + M_2, \tag{5.133}$$

where f_m^{out} represents the curvature-induced constriction force. Thus, for the bending rigidities $\kappa = 10^{-19}$ J and $\kappa = 4 \times 10^{-19}$ J, the spontaneous curvature $m = 1/(100\text{nm})$ generates the constriction forces $f_m^{out} \simeq 25$ pN and $f_m^{out} \simeq 100$ pN, respectively.

In the absence of flip-flops between the bilayer leaflets, we should include the effects of area-difference-elasticity as discussed in the previous subsection. In this case, the effective constriction force has the form

$$f_{eff}^{out} \equiv 4\pi\kappa(2m + 2m_{nlo}^{out} - M_1 - M_2) \geq 0 \tag{5.134}$$

with the nonlocal spontaneous curvature

$$m_{nlo}^{out} = \pi \frac{\kappa_\Delta}{\kappa} \frac{I_{M,0} - \mathcal{I}_M\{\Theta^{out}\}}{A} = \pi \frac{\kappa_\Delta}{\kappa} \frac{1 - r_1 - r_2}{R_{ve}} \tag{5.135}$$

as in Eq. 5.119. This term is negative, see Eq. 5.121, which implies that area-difference-elasticity acts to weaken the curvature-induced constriction forces for out-buds.

In-buds with closed necks are formed for negative spontaneous curvatures. In the latter case, we obtain the effective constriction force

$$f_{eff}^{in} \equiv 4\pi\kappa(M_1 + M_2 - 2m) > 0 \quad \text{(in-buds with } m < 0) \tag{5.136}$$

which behaves as $f_{eff}^{in} \approx f_m^{in}$ with the curvature-induced constriction force

$$f_m^{in} \equiv -8\pi\kappa m \quad \text{for } 2m \ll M_1 + M_2 < 0. \tag{5.137}$$

In the absence of molecular flip-flops between the bilayer leaflets, the effective constriction force is

$$f_{eff}^{in} \equiv 4\pi\kappa(M_1 + M_2 - 2m - 2m_{nlo}^{in}) \tag{5.138}$$

with the nonlocal spontaneous curvature

$$m_{nlo}^{in} = \pi \frac{\kappa_\Delta}{\kappa} \frac{I_{M,0} - \mathcal{I}_M\{\Theta^{in}\}}{A} = \pi \frac{\kappa_\Delta}{\kappa} \frac{1 - r_1 + r_2}{R_{ve}} \tag{5.139}$$

as in Eq. 5.119. This term is positive, see Eq. 5.122, which implies that area-difference-elasticity also acts to weaken the effective constriction forces for in-buds.

In the curvature models, a closed membrane neck is described by a point-like discontinuity of the membrane curvature. Because of the finite membrane thickness ℓ_{me}, the radius R_{ne} of the membrane neck is necessarily restricted to $R_{ne} \gtrsim \ell_{me}$. Therefore, strictly speaking, the above derivation of the effective constriction forces f_{eff}^{out} and f_{eff}^{in} implicitly assumed that $R_{ne} \gtrsim \ell_{me}$. However, we will now argue that these constriction forces may also be used to obtain a simple criterion for the cleavage of the membrane neck.

[10] The same approach has been used for the endocytosis and exocytosis of nanoparticles in (Agudo-Canalejo and Lipowsky, 2016).

Neck cleavage represents a topological transformation from a budded vesicle that has the same topology as a single sphere to a cleaved state with the topology of two spheres. The free energy difference between the budded and the cleaved state involves a contribution from the Gaussian curvature modulus κ_G, see Section 5.10 at the end of this chapter. Furthermore, this free energy difference depends strongly on the magnitude of the spontaneous curvature. For large values of $|m|$, the fission process is exergonic and reduces the free energy of the vesicle as explained in Section 5.10.3. Therefore, in the presence of a large spontaneous curvature, thermodynamics allows fission to occur spontaneously, i.e., without any free energy input from a chemical reaction such as ATP hydrolysis. How fast this exergonic process occurs depends, however, on the free energy barrier between the budded and the cleaved state of the vesicle membrane.

In order to cleave the membrane neck, we have to create two bilayer edges. For a neck with radius R_{ne}, these two bilayer edges have the combined length $4\pi R_{ne}$. The associated edge energy E_{ed} depends on the edge tension λ_{ed} and has the form

$$E_{ed} = 4\pi R_{ne}\lambda_{ed} \quad \text{with } R_{ne} \gtrsim \ell_{me} \tag{5.140}$$

where the latter inequality reminds us that the neck radius should exceed the membrane thickness ℓ_{me}. The edge energy provides a simple estimate for the free energy barrier between the budded and the cleaved state of the vesicle membrane. This barrier has to be overcome by the mechanical work $f_m R_{ne}$ expended by the curvature-induced constriction force $f_m = f_m^{out}$ or f_m^{in} from $R_{ne} = \ell_{me}$ to $R_{ne} = 0$. Therefore, we obtain the cleavage criterion $f_m R_{ne} \gg E_{ed}$ which is equivalent to

$$|m| \gg |m^{cl}| \equiv \frac{\lambda_{ed}}{2\kappa} \quad \text{for large } |m|. \tag{5.141}$$

This criterion predicts that the membrane neck is cleaved and undergoes fission if the absolute value $|m|$ of the spontaneous curvature is sufficiently large and exceeds the threshold value $|m^{cl}| = \lambda_{ed}/(2\kappa)$.

The main contribution to the edge tension λ_{ed} comes from the interface between the hydrophobic core of the bilayer and the aqueous solution. The corresponding interfacial tension Σ_{hc} may be reduced by a rearrangement of the head groups along the bilayer edge or by the adsorption of edge-active molecules. For an interfacial tension $\Sigma_{hc} \gtrsim 1$ mN/m and a thickness $\ell_{hc} \simeq 2$ nm of the hydrophobic core, we obtain the estimate $\lambda_{ed} = \Sigma_{hc}\ell_{hc} \gtrsim 2$ pN. Using the typical bending rigidity $\kappa = 10^{-19}$ J, neck cleavage requires the spontaneous curvature m to exceed the threshold value $|m^{cl}| \gtrsim 1/(100\ \text{nm})$. As we will see in Section 7.5 below, neck cleavage is further facilitated by the adhesion of membranes to solid substrates and nanoparticles.

Curvature-induced budding and fission has been recently observed in molecular dynamics simulations of nanovesicles (Ghosh et al., in preparation). In this case, the spontaneous curvature was generated by the adsorption of small solute particles. Combined budding and fission has also been observed experimentally for giant vesicles exposed to polyhistidine-tagged GFP proteins that were bound to certain lipid components within the vesicle membranes (Steinkühler et al., in preparation).

5.5.5 VESICLE SHAPES WITH SEVERAL BUDS

Let us now consider multi-sphere vesicles that consist of more than two spheres connected by more than one closed neck, see also Box 5.2. The Euler-Lagrange Eq. 5.70, which applies to all membrane segments of such a multi-sphere vesicle apart from the closed necks, implies that at most two different types of spheres with two distinct radii, $r_1 = R_1/R_{ve}$ and $r_2 = R_2/R_{ve}$, can coexist on the same vesicle.

These two radii are determined by the membrane area $A = 4\pi R_{ve}^2$, by the vesicle volume $V = v(4\pi/3)R_{ve}^3$, and by the numbers N_1 and N_2 of the two types of spheres. If both types of spheres have a positive mean curvature, the two radii r_1 and r_2 satisfy the geometric relations

$$N_1 r_1^2 + N_2 r_2^2 = 1 \tag{5.142}$$

and

$$N_1 r_1^3 + N_2 r_2^3 = v \quad (\bar{M}_1 > 0 \text{ and } \bar{M}_2 > 0). \tag{5.143}$$

If we define the volumes v_1 and v_2 of the individual spheres via

$$\frac{4\pi}{3}R_1^3 = v_1\frac{4\pi}{3}R_{ve}^3 \quad \text{and} \quad \frac{4\pi}{3}R_2^3 = v_2\frac{4\pi}{3}R_{ve}^3, \tag{5.144}$$

the relation Eq. 5.143 can be rewritten in the form

$$N_1 v_1 + N_2 v_2 = v. \tag{5.145}$$

Simple examples for such multi-sphere shapes with $N_1 = 1$ are shown in Figure 5.18a–c. If the r_1- and r_2-spheres have positive and negative mean curvature, respectively, multi-sphere shapes with $N_1 > 1$ are impossible because they would require different types of necks with positive and negative neck curvature. Therefore, we are left with $N_1 = 1$, i.e., one large sphere with N_2 in-buds as illustrated in Figure 5.18d. In the latter case, the second geometric relation Eq. 5.143 is replaced by

$$r_1^3 - N_2 r_2^3 = v_1 - N_2 v_2 = v \quad (\bar{M}_1 > 0 \text{ and } \bar{M}_2 < 0). \tag{5.146}$$

In contrast to these geometric relations, the stability relations for the membrane necks are local and do not depend on the sphere

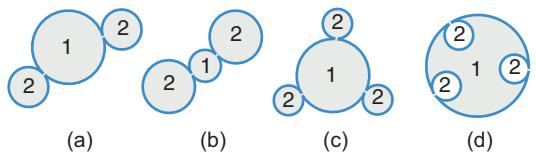

Figure 5.18 (a–c) Examples for vesicles consisting of 1 + N spheres with positive neck curvature: (a) Large r_1-sphere with two smaller r_2-spheres; (b) Small r_1-sphere with two larger r_2-spheres as observed in (Lipowsky and Dimova, 2003); (c) Large r_1-sphere with three smaller r_2-spheres; and (d) Example for a vesicle consisting of 1 + 3 spheres with negative neck curvature. For simplicity, all membrane necks have been placed in the plane of the figure. The positions of these necks are, however, arbitrary and can be shifted along the surface of the large sphere as long as the buds do not intersect each other.